Bioprinting with bioactive glasses: a review on material design, biological performance and tissue engineering applications

Acta Biomaterialia 217 (2026) 1–20

Contents lists available at ScienceDirect

Acta Biomaterialia

journal homepage: www.elsevier.com/locate/actbio

Review article

Bioprinting with bioactive glasses: a review on material design, biological performance and tissue engineering applications

Maria Erato Pianou [a,1], Andreea Luiza Mîrț [b,c,1], Valentina Rigano [a,1], Enrica Verné [a], Francesco Baino [a,*], Aldo R. Boccaccini [b,*]

[a] Institute of Materials Physics and Engineering, Department of Applied Science and Technology, Politecnico di Torino, 10129 Torino, Italy
[b] Institute of Biomaterials, University of Erlangen-Nuremberg, 91058 Erlangen, Germany
[c] National University of Science and Technology Politehnica Bucharest, 313 Spl. Independentei, 060042 Bucharest, Romania

ARTICLE INFO

Keywords:
Bioactive glasses
Bioprinting
Bioinks
Scaffolds
Tissue engineering
Nanoparticles

ABSTRACT

Tissue engineering and regenerative medicine have shown invaluable promises for the repair, recovery or replacement of diseased tissues and organs. Merging the paradigms of these disciplines with additive manufacturing technologies has recently yielded the advent of bioprinting, i.e. the layer-by-layer production of tissue-like porous scaffolds incorporating living cells. While soft biocompatible hydrogels are the ideal matrix for hosting and preserving cells during the printing process, small amounts of additional ingredients (organic or inorganic) can be incorporated in the bioinks to stimulate cell activity and impart extra-functionalities to the overall bio-printed construct. In this regard, bioactive glasses promote cell-matrix interaction and cell biology pathways through the local release of biologically active ions and are also able to elicit a local antibacterial effect which is key to combat post-surgical infections at the bioimplant site. This review aims to provide an up-to-date overview of the use of silicate, borate and phosphate glasses as valuable additives to bioinks for bioprinting applications. Opportunities for further research are highlighted and the challenges that must be tackled to advance this emerging field are discussed.

Statement of Significance: The biofabrication of a truly functional living tissue or organ in the lab for implantation in the body is one of the grand challenges of regenerative medicine. This hope has materialized with the advent of bioprinting, which allows the incorporation of living cells in a soft supportive matrix by applying additive manufacturing technologies. This review summarizes the state-of-the-art of bioprinting with bioactive glass particles incorporated in the printable ink. The current limitations and the latest evolutions in this exciting field of research are critically examined, and the roles of design parameters (e.g. composition, concentration and size of the bioactive phase) as well as the rheological, mechanical, biological and overall functional performance of such special types of bioinks are detailed. Existing results and new horizons are discussed for providing a comprehensive picture that may be useful for both experienced and early-stage researchers in the biomaterials community.

1. Introduction

Tissue engineering (TE) is an interdisciplinary field that integrates biological knowledge with advanced material design to restore or regenerate damaged tissues [1–4]. TE usually requires 3D structures (scaffolds) that provide support for the attachment and proliferation of target cells as well as the growth of newly-formed tissue, thus promoting tissue healing and regeneration [5].

Scaffolds made from engineered biomaterials play a central role in TE, being designed to support cell attachment, proliferation and tissue regeneration. Apart from the basic requirement of biocompatibility, an ideal scaffold must exhibit a combination of properties tailored to its specific application, including sufficient mechanical strength to support physiological loads as well as high (typically >60-70%) and inter-connected porosity to facilitate cell infiltration and nutrient transport to ensure integration with host tissue [5–7]. Another requirement is

* Corresponding authors.
E-mail addresses: francesco.baino@polito.it (F. Baino), aldo.boccaccini@fau.de (A.R. Boccaccini).
[1] These authors contributed equally to the work and share first co-authorship.

https://doi.org/10.1016/j.actbio.2026.05.010
Received 19 December 2025; Accepted 7 May 2026
Available online 8 May 2026

controlled dissolution/biodegradability, so that the scaffold can be gradually resorbed post-implantation leaving space to newly-formed tissue [5,6,8]. Depending on the anatomical location and mechanical demands of the target tissue, scaffolds should meet additional requirements such as shape adaptability, surface properties (e.g. topology, micro-/nano-roughness) and mechanical rigidity or flexibility [9–12].

Both the fabrication technologies and the (bio)materials used for making scaffolds continue to be areas of intensive research worldwide [13–15]. Additive manufacturing (AM), which covers a range of technologies including 3D printing, has emerged as a transformative approach in TE, enabling the precise fabrication of complex and biologically relevant 3D structures [16,17]. This technology allows producing scaffolds with highly controlled internal architectures and shows great promise in implant customization using patient-specific models [18,19]. Since Chuck Hull first introduced the idea of AM in 1986 through stereolithography (SLA), this class of advanced fabrication strategies has found applications in many common-life and high-tech fields. Recent advances in 3D printing methods have enabled the evolution of the technology in the biomedical field [20] from material-centered prototyping to the biofabrication concept, which involves the direct incorporation of living cells into printable hydrogels (bioinks) [21,22]. 3D bioprinting, as a popular approach in the biofabrication field, enables the fabrication of cell-laden constructs with controlled mechanical properties, biological functionality and complex tissue-mimicking 3D architecture [23,24], thereby ultimately supporting a more effective tissue regeneration [25,26].

A key aspect of 3D bioprinting concerns the selection and design of bioinks, which must balance printability, mechanical strength, and biocompatibility to support cell viability during printing and tissue maturation after bioprinting. Despite the significant progress in 3D bioprinting [27–29] in terms of bioink design and technologies, there are still challenges in optimizing bioprinting resolution, mechanical stability, and long-term cell viability/overall functionality of the bioprinted constructs [30,31]. Therefore, significant research efforts are being devoted to this field, with research aiming to refine the design and formulations of bioinks and improve printing technologies [32,33]. While various “soft” organic materials such as synthetic thermoplastics (e.g., polycaprolactone (PCL)) and decellularized matrices (dECM) can be utilized in bioprinting as components of the bioink, hydrogels are the most promising matrix due to multiple reasons. In fact, hydrogels offer a unique combination of high permeability and a hydrated environment that support cell viability [22,34]. Furthermore, when incorporating bioactive inclusions such as ceramic or glass particles, hydrogels serve as a critical rheological controller, providing the necessary viscosity to maintain inorganic particles in suspension while enabling precise deposition during the printing process of the composite bioink [29, 35–37]. In this context, addition of inorganic biodegradable or bioreactive fillers, such as bioactive glasses (BGs), has gained attention recently [38]. This review summarizes the current state of the art in this specific area of multimaterial hydrogel-based bioink development, discussing the different BG compositions explored, their cell biology impact and the properties of the obtained 3D-printed structures for applications in TE and in the development of 3D tissue models.

2. Fundamentals of BGs and bioprinting

2.1. Synthesis of BGs

BGs are among the most useful materials for TE applications due to their outstanding properties, including great compositional versatility, broad-spectrum bioactivity and potential for multiple therapies (e.g. simultaneous stimulation of target cells, angiogenesis, antibacterial and immunomodulatory response) [39–41]. The first BG, having the composition $45SiO_2$-24.5CaO-24.5Na_2O-6P_2O_5 (wt.%) (“45S5 Bioglass”), was reported by Hench in 1971 [42] and has been mostly considered for orthopedic and bone tissue applications.

BGs are typically produced by melt-quenching or sol-gel synthesis. While sol-gel synthesis allows fabrication at lower temperatures, provides more control over the glass composition and carries the option of having mesopores inside the material; melt-quenching requires rapid cooling from high temperatures (typically 1200-1500°C) to obtain amorphous (non-crystalline) products. The latter method is typically faster than sol-gel synthesis to obtain the final material (half a day vs. several days [43]) and has a significantly higher yield in terms of mass of material produced per working cycle. On the other hand, nano-sized BG particles can be directly obtained by sol-gel method without any further processing. While sol-gel synthesis follows a “bottom-up” approach allowing for precise control over nanoparticle diameter during chemical gelation, melt-quenching is inherently a “top-down” process. In order to obtain fine particles from a melt-derived glass frit, intensive mechanical post-processing is required, e.g. long-term milling procedures [44]. More recently, an alternative method based on the flame spraying technique has been also proposed to directly synthesize BG particles in the nanoscale size range [45]. In terms of textural features, mesoporous sol-gel BGs have a larger specific surface area compared to melt-derived BGs, which makes the ion release and hydroxyapatite (HA) formation faster, which is important for bone TE applications since both can improve the bone-bonding and osteogenic effect of the scaffolds [46].

2.2. Bioactivity and cellular interactions of BGs

BGs demonstrate surface bioactivity by creating a layer of nanocrystalline HA when in contact with body fluids, which is of fundamental importance to improve osseointegration of an implant to the host living bone [47]. Several variants of the 45S5 BG parent composition or even totally new BG systems have been proposed and characterized over the years to provide customized properties, like better mechanical properties, targeted degradation rates or extra-functionalities like antibacterial activity and angiogenic effects [48–50]. In this regard, BGs allow the in-situ release of biologically active ions, depending on the specific material formulation. The emerging field of ionic medicine, specifically ion assisted TE, uses these ions therapeutically to promote and guide healing, thereby carrying an invaluable potential for advancing regenerative medicine [51,52]. In this context, not only silicate BGs are developed and applied but also bioactive systems based on phosphate and borate glasses. Because of their capability to form bonds with both hard and soft tissues, over the last decade BGs have been proposed in emerging fields of regenerative medicine and TE (e.g. soft tissue repair) beyond their traditional applications in contact with bone and teeth [53,54]. For example, one commercial product based on the borate 13-93B3 glass composition (53B_2O_3–6Na_2O–12K_2O–5MgO–20CaO–4P_2O_5, wt.%) (Mirragen®, ETS Engineered Tissue Solutions, USA) has been cleared by U.S. Food and Drug Administration for use as fibrous mats in wound healing and skin repair [55].

When cells are encapsulated within a 3D hydrogel matrix, they reside in an environment that mimics native tissue through the hydrogel high water content and network permeability, which are essential for nutrient exchange and cell migration [56]. By incorporating BG particles into this system, the hydrogel is transformed into a localized ionic microenvironment. Within this hydrated architecture, the glass phase slowly dissolves and releases therapeutic ions, which can trigger specific cellular responses (osteogenesis, angiogenesis, etc.) or provide crosslinking agents [41]. These ions mediate intracellular signaling pathways in diverse cell types, triggering specific pathways for new tissue formation and blood vessel growth without the need for expensive external growth factors. From a translational perspective, the choice of a cell model is crucial when evaluating BG-based bioinks. While immortalized cell lines (e.g., MC3T3-E1) are frequently used to provide reproducible data for printability and cytotoxicity studies [57,58], they may not fully capture the complex biological responses of primary human tissues. To address translational relevance, bone marrow-derived mesenchymal stem cells (BMSCs) and adipose-derived stem cells (ASCs) are the most

promising candidates. In particular, ASCs offer relative ease of isolation and a pro-angiogenic synergy with BGs [59,60], while BMSCs remain the standard for bone-specific regeneration [61,62].

Nevertheless, a major challenge in biopriting remains the fundamental trade-off between biological stimulation and cellular stress. While ion release is necessary for tissue repair, it must be carefully controlled to avoid pH instability and cytotoxic effects. Therefore, the key to successful bioink formulation lies in identifying an optimal BG concentration that maximizes its benefits to ensure safe and effective bioink formulations for tissue regeneration [38,63].

2.3. BGs into printing platforms

Glass powder obtained from glass frit milling or sol-gel processes (which can range from the nanoscale to microparticles and granules) can be used as a starting material for making scaffolds. BG scaffolds can be fabricated using a variety of methods, either conventional (e.g. sponge replication [64] and sol-gel foaming [65]) or based on electrospinning [66] and AM technologies, such as selective laser sintering [67] and extrusion-based fabrication [68–70].

In addition to scaffolds made purely from BGs, BG particles have also been incorporated into hybrid biomaterials and composites such as cell-laden hydrogels and microcapsules to enhance biological properties. For example, Sarker et al [71] and Reakasame et al [72] developed alginate–keratin and alginate dialdehyde–keratin microcapsules containing 45S5 BG particles using a pressure-driven extrusion technique to encapsulate MG-63 cells, achieving positively improved bioactivity and sustained cell viability over 21 days. Similarly, Rahimnejad et al [73] encapsulated L929 fibroblasts within chitosan-based microbeads containing BG particles, reporting metabolic activity and early HA formation on the bead surfaces.

Extrusion-based methods are commonly used in bioprinting, which usually involves the 3D printing of cell-laden hydrogels [38]. The process relies on the continuous deposition of cell-laden strands extruded through a micro-nozzle, driven by pneumatic or mechanical pressure [74], a simple scheme of this approach is displayed in Fig. 1. A critical requirement for this process is non-Newtonian shear-thinning behavior of the bioink, e.g. the bioink must decrease in viscosity under the high shear rates found inside the nozzle to allow for smooth flow, and then rapidly recover its viscosity upon deposition to maintain the shape fidelity of the printed 3D construct [75]. In extrusion-based bioprinting, the fundamental challenge is thus achieving a balance between low-pressure extrudability and high shape fidelity. While basic hydrogels often lack the structural integrity to maintain 3D architecture post-deposition, the incorporation of BGs act as a critical rheological modifier. Representative examples of this strategy include reinforcing natural-derived matrices such as gelatin methacryloyl (GelMA) and alginate dialdehyde–gelatin (ADA-GEL) with BG nanoparticles for mechanical stability, often integrated with biological signals such as growth factors (for example, bone morphogenetic proteins (BMPs)) as well as engineered DNA-based bioinks [76–78]. Additionally, advanced methods like multiport chaotic bioprinting offer a way to fabricate complex, multilayered BG containing hydrogel architectures with the high spatial organization required for functional, vascularized tissue models [37]. Indeed, the fabrication and characterization of cell-laden scaffolds that satisfy the structural, mechanical and biological needs of target tissues is at the center of biofabrication efforts worldwide [31, 79–81].

Studies dealing with the addition of BGs in particulate form, mainly melt-derived dense or gel-derived mesoporous nanoparticles, to bioprintable inks are increasingly emerging. Given the potential of the synergies at the interface of biomaterials science, advanced manufacturing, chemistry and biology, an explorative review of the literature focusing on these emerging applications and challenges thereof appear both timely and important. This review thus updates and expands previous work [82] on the topic of BG-containing bioinks. While most studies have focused on applications in bone TE, recent reports have also indicated emerging applications of BG-containing bioinks in other TE and biofabrication branches, including the development of tissue mimicking 3D models, which will be discussed in the present work.

3. Bioprinting using pure silica nanoparticles (as borderline case of BGs)

Among inorganic fillers used in bioinks, silica nanoparticles have been analyzed as a promising biomaterial inclusion for improving the mechanical and biological properties of bioprinted scaffolds. Amorphous pure-silica materials can be considered a borderline case of silicate glasses entirely constituted by SiO_2. According to the seminal study by Wilson et al [83], who fixed the “bioactivity threshold” at 60 mol.% of SiO_2, pure silica systems should not be inherently bioactive in the traditional sense, meaning that they do not spontaneously form a HA layer when in contact with physiological fluids, e.g. simulated body fluid (SBF); however, their interaction with SBF ions can still lead to HA formation under certain conditions. This “indirect” bioactivity is especially observable in mesoporous silica materials, where ultra-high surface area and pore volume facilitate ion exchange and surface reactions

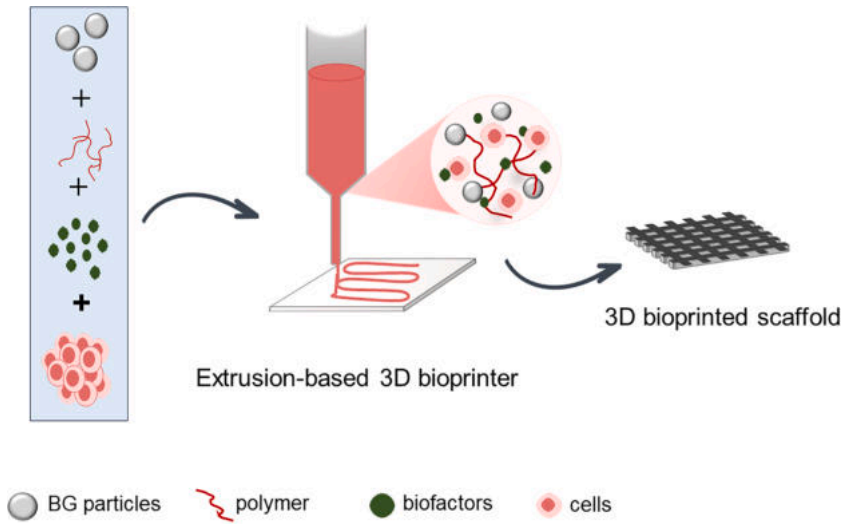

Fig. 1. Concept of bioprinting using BG (nano)particles as bioreactive additive in bioinks for producing cell-laden scaffolds.

in contact with physiological fluids [84,85]. The presence of surface silanol (Si–OH) groups serves an important function as these sites can adsorb calcium and phosphate ions from biological fluids through hydrogen bonding, thereby initiating nucleation and growth of HA [86]. At present, just a few publications have been found in the literature about the incorporation of silica nanoparticles, in very low amounts, in printable bioinks, as discussed in this section.

For example, Sun et al [77] incorporated mesoporous silica nanoparticles (MSNs) in a concentration of 0.4-0.8% w/v into bioinks leveraging their open-pore structures and optimal pore sizes for entrapping biomolecules and, specifically, exploiting the MSNs capacity to load BMPs in order to ensure continuous release within the scaffold [87,88]. The slurry created for 3D-bioprinting consisted of gelatin, gelatin methacryloyl (GelMA), four-arm poly(ethylene glycol) (PEG) acrylate, lithium phenyl-2,4,6-trimethylbenzoylphosphinate (LAP) as a photoinitiator and MSNs loaded with BMP-4. Additionally, two types of cells were incorporated: BMSCs from rats (180-200 g) and RAW264.7 cells (cell line isolated from a mouse tumor). The resulting bioink was used to fabricate scaffolds through an extrusion-based method with a 3D-Bioplotter. MSNs had an average particle size of 139.7 nm and a mesopore size of 8.9 nm, making them suitable for loading BMPs [89]. The overall porosity of the scaffolds was not affected by the presence of the silica inclusions, as a very small amount of MSNs was used. On the other hand, the addition of silica nanoparticles influenced the viscosity of the bioink, which became higher with increasing MSN concentration (Fig. 2a). Furthermore, higher MSN content improved print resolution, shear-thinning behavior and compressive strength (Fig. 2b). Post-printing cell viability was assessed using the Live/Dead and Cell Counting Kit-8 (CCK-8) assays, revealing that over 90% of cells survived after 24 hours with robust proliferation (Fig. 2c). In vivo studies in rat calvarial defect models further demonstrated significantly enhanced bone regeneration in the BMSC/RAW/BMP-4 group, which contained BMP-4-loaded MSNs. Micro-CT analysis performed after two months included quantitative evaluation of bone volume fraction and bone mineral density, revealing markedly higher values in the MSN-containing group compared to BMSC, BMSC/BMP-4, and BMSC/RAW controls (Fig. 2d). These findings indicate that BMP-4 released from MSNs effectively induced BMSCs differentiation and promoted macrophage polarization, enhancing both osteogenesis and angiogenesis. The study thus convincingly demonstrated the essential contribution of MSN addition to the success of the bioprinting approach.

Lee et al [63] utilized commercially-available silica nanoparticles (SiNPs), modifying them into aminopropyl-functionalized silica nanoparticles (AmMPs), at low concentrations to achieve a negative zeta potential (cationic). The bioink was formulated using anionic polymers and cationic AmMPs in order to enhance print fidelity and mechanical strength. Specifically, the bioink comprised alginate (3% w/v) and gellan (3.5% w/v), AmNPs and bovine chondrocytes isolated from bovine knee articular cartilage. The cell suspension (1×108 cells/mL) was incorporated into the ink at 1:9 (v/v) ratio. It was shown that the inclusion of silica nanoparticles increased the zero-shear viscosity of the bioink by 1062% compared to the control ink without nanoparticles (Fig. 3a). Additionally, at low nanoparticle concentration (2 wt.%), no significant change in the storage modulus was observed; however, beyond 4 wt.% a marked increase was noticed (Fig. 3b). The formulated slurry was then extruded using a 3D printer. A comparison between the bioink with and without silica nanoparticles revealed that the former exhibited partial pore closure during and after the printing process, whereas the latter maintained open pores upon the addition of AmPNs (Fig. 3c). A cell viability assay demonstrated ~90% viability after four

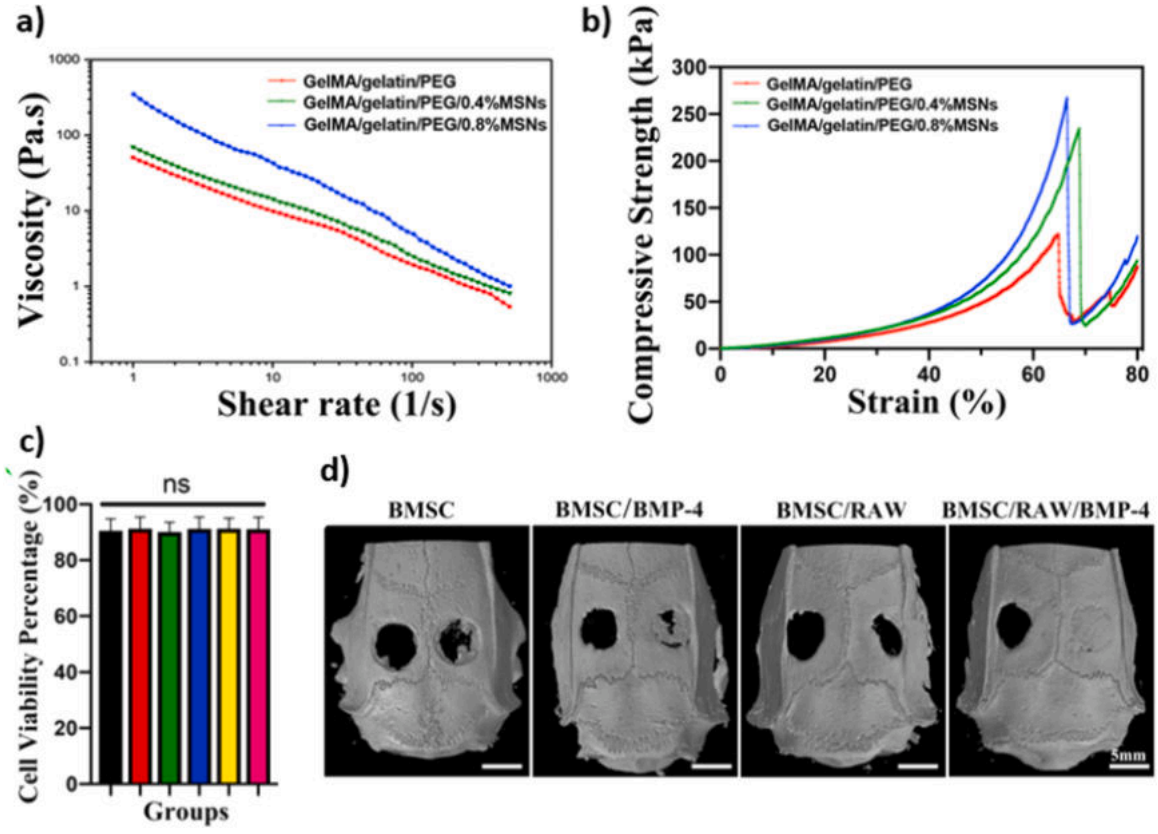

Fig. 2. Summary of results on 3D bioprinted scaffolds based on GelMa, gelatin and PEG containing MSNs: (a) viscosity as a function of shear rate at 20°C; (b) compressive stress-strain curves; (c) cell viability percentage of scaffolds from different groups with loading of RAW macrophages and/or BMSC; (d) 3D reconstruction of micro-CT images; the scaffolds were implanted in the right side. Reproduced from Ref.[77] with permission from Elsevier on behalf of KeAi Communications Co., Ltd.

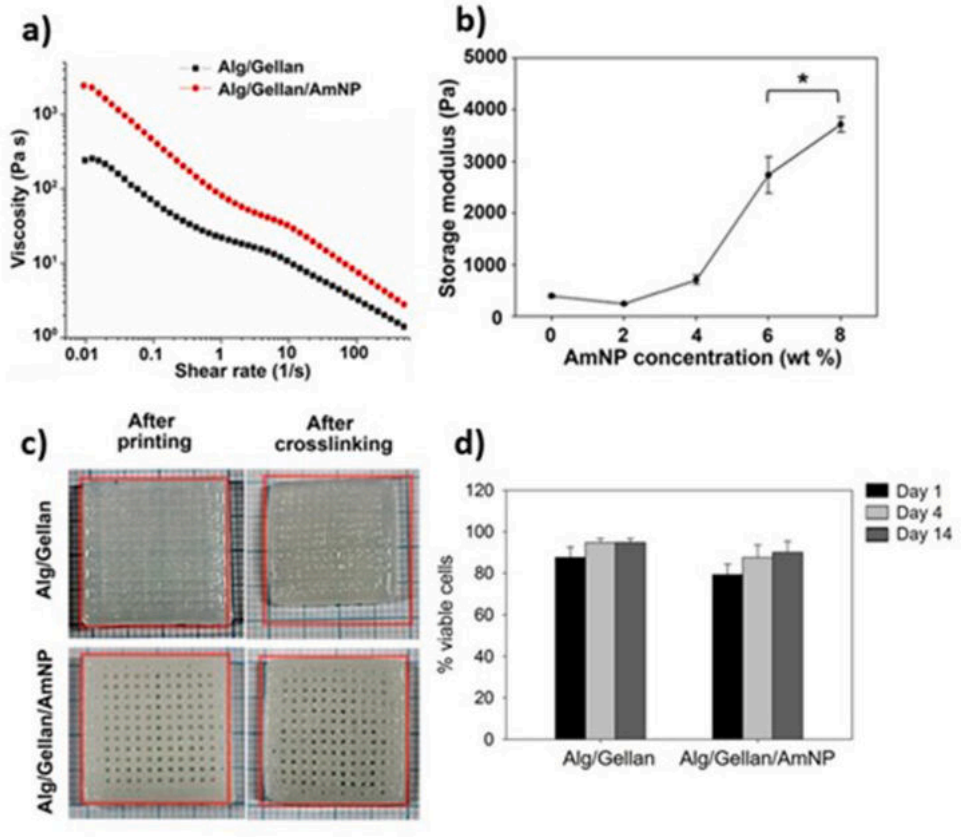

Fig. 3. Summary of results on 3D bioprinting of alginate-gellan gum mixture containing AmMPs: (a) viscosity properties of inks and cross-linked hydrogels; (b) storage modulus of Alg/gellan inks with different amounts of AmNP; (c) images of printed 10-layered grids (2 × 2 cm^2) before and after cross-linking; (d) viability of cells encapsulated in each ink without extrusion. Reproduced from Ref.[63] with permission from ACS.

days, regardless of the presence of AmNPs (Fig. 3d).

Tavares et al [90] developed photocrosslinkable GelMA-based bioinks incorporating MSNs functionalized with calcium, phosphate and dexamethasone (MSNCaPDex) [91]. These nanocomposite bioinks, laden with human bone marrow-derived mesenchymal stem cells (hBM-MSCs), were successfully processed into structurally stable 3D-bioprinted constructs, achieving uniform nanoparticle dispersion throughout the hydrogel matrix. In this work, hBM-MSCs, cultured in basal medium, were suspended in GelMA solutions at a final cell density of 4 × 10^6 cells/mL. The bioink formulation, comprising 10% GelMA, 0.5% MSNCaPDex, and 0.1% Irgacure 2959, was prepared at 37 °C and cooled on ice to optimize viscosity prior to printing. Bioprinting was conducted at room temperature under varying pressures, with the printhead temperature maintained in the range 20–21 °C. Cell viability was assessed through live/dead staining at 1, 7 and 14 days post-printing, revealing high levels of viable, well-distributed cells throughout the constructs, and sustained cell viability across the entire culture period.

The studies considered above confirmed the potential of using silica nanoparticles in bioprinting, with different target applications. For example, Lee et al [63] and Tavares et al [90] focused on improving the printability and mechanical stability of bioinks, while Sun et al [77] explored the biofunctional role of MSNs (as growth factor delivery vehicles) in tissue regeneration. These findings collectively indicate that silica nanoparticle-modified hydrogels can serve the dual function of enhancing mechanical and rheological properties of bioinks as well as their biological activity, thereby broadening the scope of MSN-containing bioinks for bioprinting applications in cartilage and bone TE.

4. Bioprinting using multicomponent glasses

4.1. Bioprinting with silicate BGs

Bioprinting with multicomponent silica-based BGs has emerged as a promising approach for developing bioinks that can enhance the mechanical integrity of the scaffold, as well as the cell viability and bioactivity. Specifically, BG nanoparticles have demonstrated a great potential in promoting osteogenesis, facilitating biomineralization and improving scaffold osteo-integration [38]. Among them, mesoporous BGs (MBGs) are highly appealing as, exhibiting an inherent nanoporous texture, they can uptake and release growth factors and drugs besides delivering bioactive ions, thus synergistically potentiating the overall therapeutic effect [92,93].

In an early study, Gao et al [94] used commercial 45S5 BG (particle size 20 μm) and HA (particle size < 200 nm) with bone marrow-derived human mesenchymal stem cells (hMSCs) incorporated into a poly (ethylene glycol) dimethacrylate (PEGDMA) hydrogel scaffold fabricated via thermal inkjet printing. While BG incorporation reduced hMSC viability compared to HA, it enhanced early osteogenic marker expression (RUNX2), indicating strong osteoinductive potential. In contrast, HA supported higher cell viability and promoted extracellular matrix formation and osteogenic differentiation, which was consistent with an elevated alkaline phosphatase (ALP) activity and collagen production. In summary, this study showed that PEG-based hydrogels containing bioactive ceramic particles can be bioprinted to create constructs for the regeneration of the osteochondral interface.

Several studies have also explored the use of sol-gel derived BG nanoparticles (BGNPs) doped with various ions to enhance osteogenic potential. Extrusion-based bioprinting with sol-gel BG nanoparticles was first explored by Leite et al [95] who investigated the incorporation of

strontium (Sr), a well-known anti-resorption agent for bone tissue as well as a stimulator of osteogenesis and in vitro bone formation [96]. In this study, BGNPs were synthetized in a Sr-free composition (55%SiO_2–40% CaO–5%P_2O_5 mol.%), while Sr-doped nanoparticles (Sr-BGNPs) had a modified composition of 55SiO_2–30CaO–5P_2O_5–10SrO (mol.%). The particle size of BGNPs ranged from 40 to 100 nm. In order to ensure biocompatibility, low toxicity and cost-effectiveness, the bioinks were formulated using a multimodal alginate dialdehyde gelatin hydrogel (ADA-GEL), into which BGNPs or Sr-BGNPs were incorporated at low concentrations (0.1% and 0.5% w/v). MG-63 osteoblast-like cells were also embedded in the bioink. Results demonstrated that the bioink increased its viscosity with the increment in BGNP concentration. In vitro testing further revealed that, after soaking the scaffolds in SBF, a calcium phosphate (CaP) layer began to form on the material surface. Elemental analysis on the material showed an increase in calcium (Ca) and phosphorus (P) content along with a decrease in silicon (Si), indicating the concurrent formation of the CaP layer and the dissolution of BGNPs [97]. Additionally, EDS analysis and SEM micrographs performed on the constructs soaked in SBF showed that the intensity of Ca and P peaks increased with higher BGNP concentrations (Fig. 4a). Cell viability was assessed 24 hours post-printing, revealing that the number of viable cells was comparable to that in scaffolds without BGNPs. The results thus revealed that the presence of BGNPs in the printable hydrogel did not negatively affect cell survival (Fig. 4b) but promoted the local formation of a CaP phase on the bioprinted scaffolds.

Guduric et al [98] modified a MBG network by substituting calcium (Ca) with zinc (Zn), leveraging the osteoblastogenic and antimicrobial effect of zinc. MBG particles with a basic molar ratio of Si/P/Ca = 80:5:15 (mol.%), sieved to a size below 45 μm, were Zn-modified (5, 10 and 15 mol.%) and incorporated into a bioink formulation. The bioink included also a blend of alginate (alg), methylcellulose (MC) and human mesenchymal stem cells (MSCs) with a density of 1×10^6 cells per milliliter. In order to assess rheological properties, bioinks with different Zn-doped MBG concentrations (0, 3, 5, 7 and 10%) were prepared using two different alg-MC blends, i.e. 3-6 (3 wt.% alg and 6 wt.% MC) and 3-9 (3 wt.% alg and 9 wt.% MC). The results indicated that the increment of MBG concentration led to an increase in hydrogel viscosity. The optimal composition for mixing, rheology and printability was identified as 7% MBG (Fig. 5a). The bioinks were printed by using an extrusion-based 3D bioprinter. It was observed that inks with no or low amount of MBG particles were insufficiently viscous to maintain stable macropores during printing. The best print quality was achieved using 3-9 alg-MC blends incorporating 7% of Zn-doped MBG particles (Fig. 5b), indicating that a higher amount of MBG particle and a lower Zn concentration in the particles yielded the most structurally stable scaffolds. Post-printing cell viability in MBG-containing scaffolds was analyzed. Immediately after printing, Zn-modified scaffolds exhibited slightly reduced cell number compared to the MBG-free control. However, cell proliferation increased over three days, suggesting that MBG particle incorporation had a positive effect on cellular behavior. MBGs, like those studied in the paper, provide a customizable system for controlled ion release, enabling the sustained delivery of therapeutic agents such as antibacterial ions (e.g. silver, copper, zinc) or osteoinductive ions (e.g. calcium ions and silicon(IV) species), and bioactive molecules, e.g. growth factors or antibiotics.

Wang et al [99] also explored the use of BGNPs, employing particles with a size of 55 nm and a three-component BG with molar ratio Si:Ca:P = 66:27:7 (mol.%) in combination with an alginate and gelatin blend. In

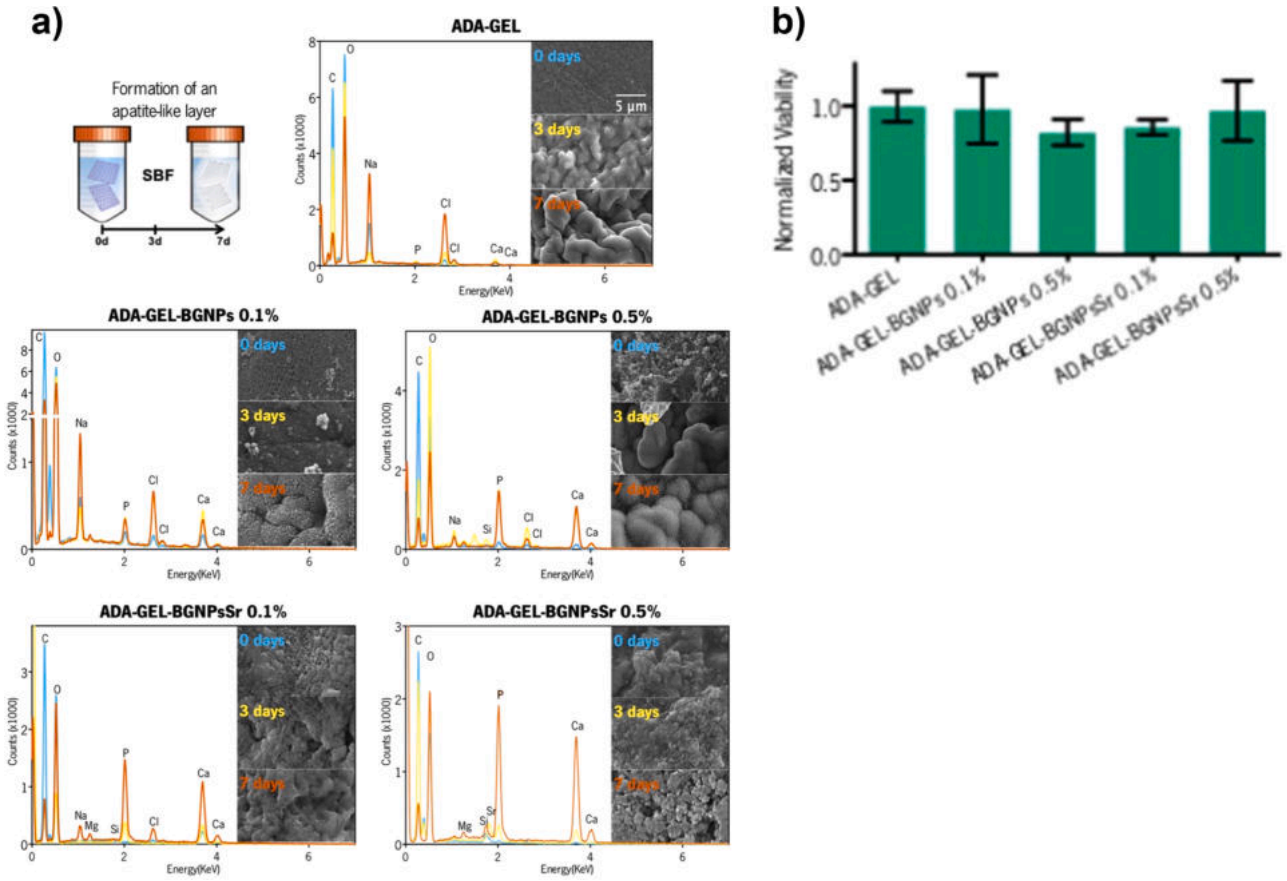

Fig. 4. Results on the characterization of ADA-GEL-BGNP composite bioink: (a) schematic representation of the in vitro bioactivity studies and characterization of the chemical elements using EDS supported by SEM micrographs of the constructs soaked in SBF solution during 0, 3 and 7 days. (b) Normalized viability of MG-63 cells after incubation for 24 h. Reproduced from Ref.[95] with permission from IOP Publishing Ltd.

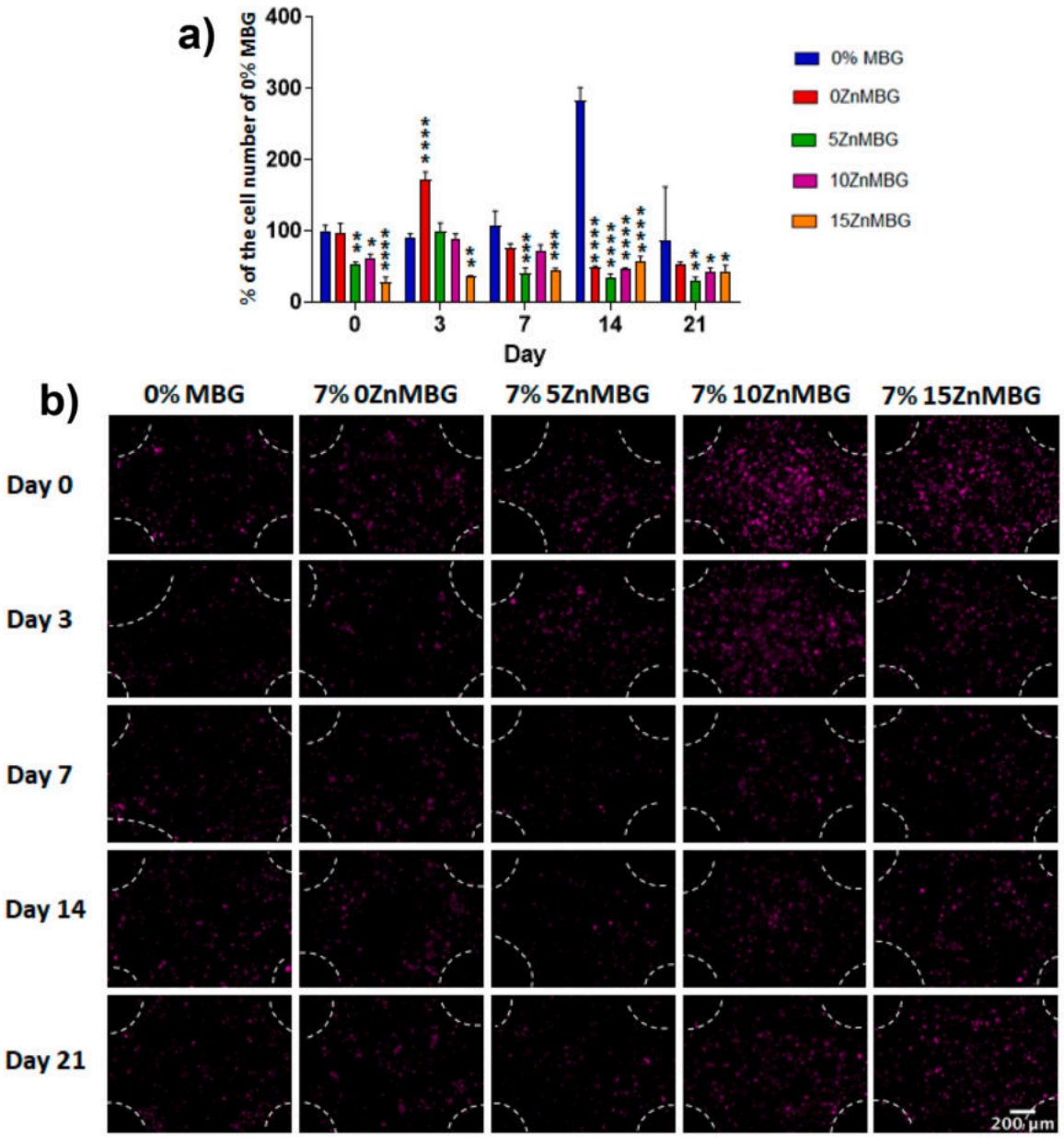

Fig. 5. Results obtained on 3D printed alginate-based scaffolds containing Zn-MBG particles: (a) development of number of MSC in bioprinted composite scaffolds during 21 days of culture examined by quantification of DNA extracted from cells encapsulated in bioprinted constructs; (b) fluorescence-microscopic images of Vibrant DiD pre-labeled MSC within bioprinted composite scaffolds during 21 days of culture. All images are taken at crossings of printed strands. White markings show the borders of printed strands and pores. Scale bar corresponds to 200 μm and the cells appear as violet spots. Reproduced from Ref.[98] under the Creative Commons Attribution (CC BY 4.0) license (MDPI).

this study, human osteosarcoma cells (SaOS-2) were incorporated in the bioink that was printed in a computer-controlled 3D printer. Post-printing elemental analysis indicated the accumulation of oxygen (O), phosphorus (P), calcium (Ca), and carbon (C), suggesting mineral deposition (hydroxycarbonate apatite formation). Additionally, the bioprinted cells exhibited increased proliferation and mineralization ability, further supporting the role of BGNPs as an effective, osteostimulatory filler material in bioprinting. Ojansivu et al [100] incorporated BG microparticles (composition: 47.12SiO_2-6.73B_2O_3-6.77CaO-22.66-Na_2O-1.72P_2O_5-5MgO-10SrO, mol.%) with a particle size of 13–50 μm into gelatin–alginate bioinks, containing human osteoblast-like cells (Saos-2 cells), to provide osteogenic effects. The addition of BG and cellulose nanofibrils (CNF) improved the rheological behavior and printability of the bioink, although higher viscosity was associated with reduced cell viability. Human bone marrow–derived stem cells demonstrated better survival and osteogenic activity than human osteoblast-like cells after printing, indicating that the bioink viscosity and shear stress during printing had significantly affected the cellular response.

Research has further demonstrated that BG-based bioinks can serve as bioactive templates that not only provide structural support but also actively promote bone tissue regeneration through controlled ion release and enhanced cellular interactions. For example, Wang et al [101] investigated the use of mesoporous bioactive glass nanoparticles (MBGNs) (80%SiO_2-15%CaO-5%P_2O_5, molar composition) as a drug delivery system, loading the nanoparticles with doxycycline (DOX). DOX had a twofold role acting as a broad-spectrum antibiotic and gene expression regulator that enhances BMP-2 production, promoting osteogenic differentiation of stem cells. This bioink formulation included DOX, MBGNs and polycaprolactone in a mass ratio of 2:10:88, along

with 5% GelMA, 1% HAMA (methacrylated Hyaluronic Acid), 0.5% LAP and murine mesenchymal stem cells (C3H10T1/2) at a concentration of 1×10^7 cells/mL. The cell-loaded bioink was printed using an extrusion 3D printer. Cell viability was assessed using cell counting Kit-8 (CCK-8), revealing a nearly fivefold increase in cell proliferation after 21 days post-printing. In vivo experiments demonstrated ectopic osteogenesis in the scaffolds, further confirming the osteoinductive potential of the DOX-loaded MBGNs. Although this study primarily focused on DOX-controlled BMP2-expressing cells, it provided valuable insights into how bioinks can be engineered for dual functionality, combining osteogenic stimulation and antimicrobial properties.

Miao et al [32] examined the use BG microspheres (BGMs) with a molar composition of 60% SiO_2, 36% CaO and 4% P_2O_5, to develop a scaffold suitable for periodontal tissue regeneration. BGMs at 5% w/v were incorporated into an ink composed of 15% w/v gelatin methacryloyl (GelMA), 10% w/v sodium alginate (SA) and 0.5% w/v photoinitiator (PI 2959). Bone marrow mesenchymal stem cells at a density of 1×10^7 cells/mL were included in the bioink, along with BMP2 and platelet-derived growth factor (PDGF), utilizing the multidirectional differentiation of stem cells. The bioink was printed layer by layer using an extrusion-based 3D printer. SEM analysis of the scaffold soaked in SBF for 3 days revealed the formation of HA exclusively in BGM-containing scaffolds (Fig. 6a); however, by the 7th day, HA deposition was also observed in BGM-free scaffolds, although in the form a thinner layer compared to the BGM containing counterpart. This trend was further confirmed by XRD analysis (Fig. 6b), demonstrating that the presence of BGM accelerated the in vitro bioactivity kinetics. Moreover, cell viability was assessed using a live/dead assay and CCK-8 analysis (Fig. 6c), both of which indicated improved cell proliferation in scaffolds containing BGMs. In vivo tests were conducted by transplanting the cell-containing scaffolds into beagle dog's periodontal defects, yielding promising results in terms of bone regeneration. These findings demonstrate significant regeneration of periodontal tissue, with a complete periodontal structure reconstructed at treated sites after just 8 weeks, which confirmed the scaffold efficacy in both soft and hard tissue repair.

The ADA-GEL hydrogel system has been intensively investigated in recent years as a printable matrix for incorporating different types of BG nanoparticles [82,102,103]. The concept has been the investigation of the effect of bioreactive fillers on the printability of the bioinks and the resultant properties of the bioprinted constructs. Heid et al [104] developed a bioink based on ADA-GEL and bioactive inorganic fillers (BIF), namely SiO_2-CaO submicrometric particles (150–400 nm), with the aim of improving printability and biocompatibility for soft TE applications. Composites with 0.1% BIF and ADA-GEL hydrogels (2.5% ADA-3.75% GEL, w/v) were used. NIH/3T3 fibroblasts were encapsulated in the bioink at a density of 1×10^6 cells/mL. The bioinks were loaded into cartridges and printed using an extrusion printer with a cooled printhead (23°C) at 5 mm/s. The constructs (15×15 mm^2 grids) revelead that strand resolution and morphology were affected by BIF content: higher BIF concentrations increased viscosity and mass flow, enabling finer strand formation at early gelation stages but leading to irregularities over time. At 30 min post-fabrication, ADA-GEL-BIF (A19GB0) scaffolds demonstrated optimal resolution (<0.5 mm), while higher BIF content (A19GB5) required increased extrusion pressures and resulted in more irregular strand deposition. Cell viability and behavior were assessed over 14 days using metabolic and live/dead assays, as well as phalloidin/DAPI staining (Fig. 7a). On day 1, all constructs showed high cell viability, with fibroblasts retaining a rounded shape. By days 2–3, cell spreading began, particularly in hydrogels with higher degree of ADA oxidation, which degraded faster and exhibited increased microporosity. Higher BIF concentrations, while stabilizing the hydrogel and increasing Ca^{2+} release, also raised pH and slowed degradation, reducing cell elongation. Pure ADA-GEL hydrogels without BIF degraded rapidly and lost structural integrity within one day of incubation. The study was important to demostrate the complex effect of ion

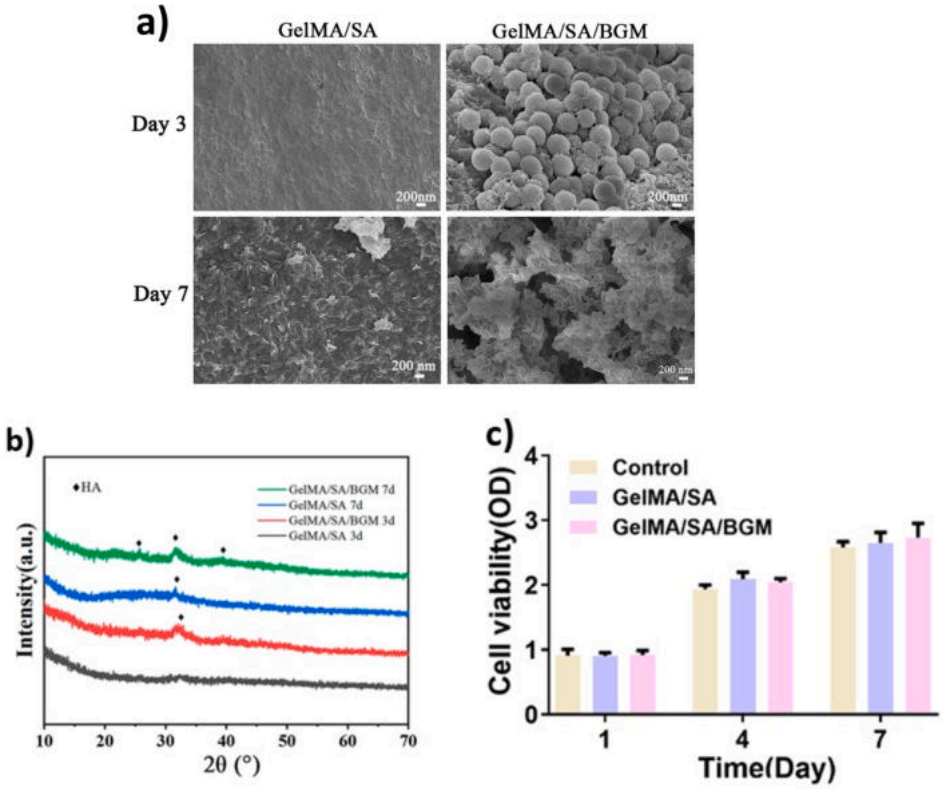

Fig. 6. Results on GelMA/SA and GelMA/SA/BGM bioprinted scaffolds with mBMSC cells: (a) SEM images (scale bars 200 nm) and (b) XRD patterns of GelMA/SA and GelMA/SA/BGM after immersing in SBF for 3 and 7 days. (c) Cell proliferation viability after culturing with GelMA/SA and GelMA/SA/BGM. Reproduced and adapted from Ref.[32] under the Creative Commons Attribution (CC BY 4.0) license (MDPI).

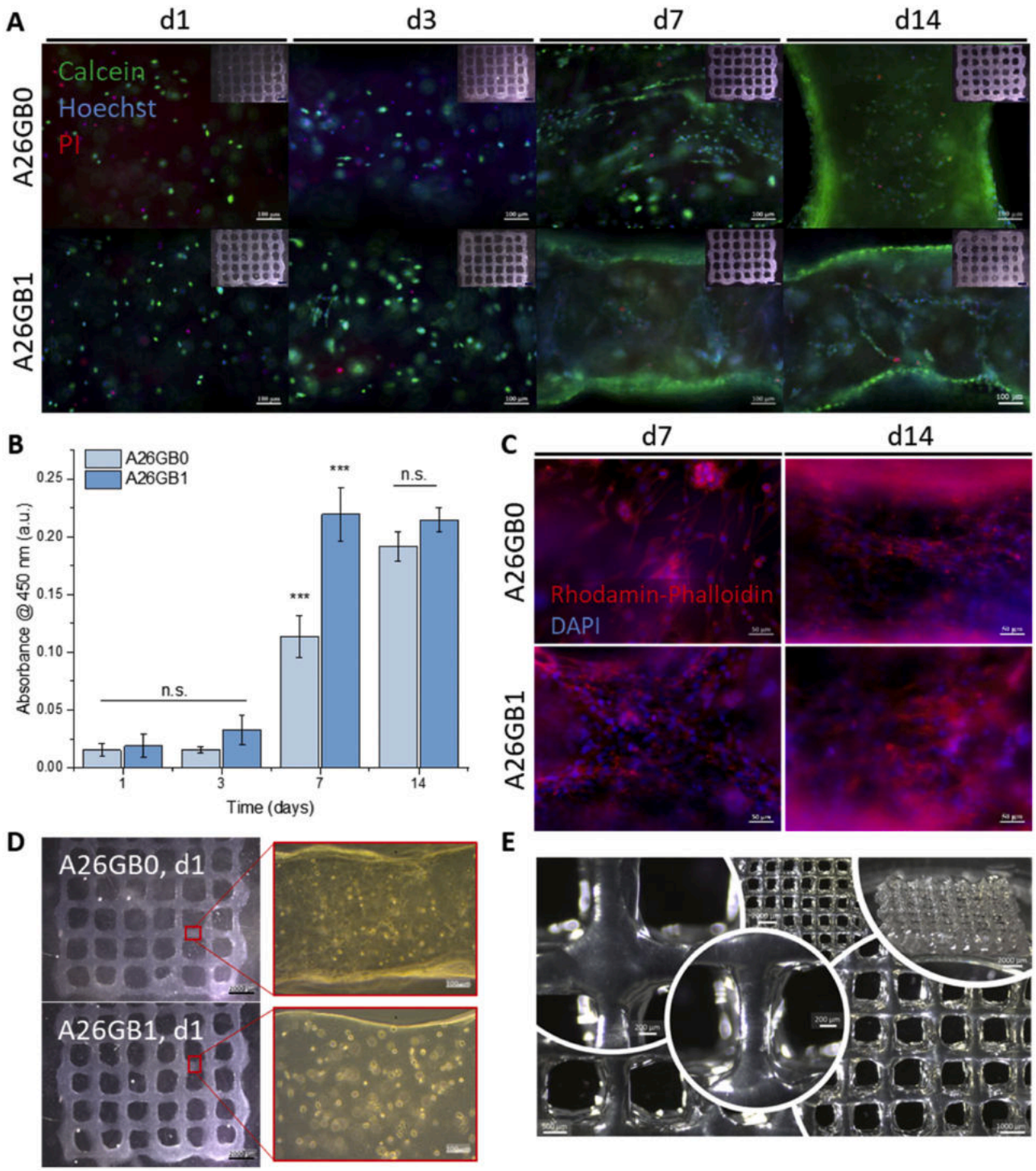

Fig. 7. Assessment of bioprinted ADA-GEL/BIF (SiO_2-CaO particles): (A) live/dead staining showing cell viability over 14 days (all scale bars correspond to 100 μm); (B) mitochondrial activity via WST-8 assay; (C) cytoskeletal organization on days 7 and 14 (all scale bars correspond to 50 μm); (D) cell distribution post-printing (scale bars on the left side 1000 μm, scale bars on the right side 100 μm); (E) 3D printed grid structures with high shape fidelity (scale bars: top left 200 μm, bottom left 500 μm, top center 2000 μm, center 200 μm, top right 2000 μm, bottom right 1000 μm). Adapted and reproduced from Ref.[104] with permission from Elsevier.

(Ca)-releasing BIF on both printability and long term degradation behaviour of the printed constructs in addition to the biological influence of local Ca and Si release from the included BIF (Figs. 7b-e).

More recently, Lu et al [105], tested ADA-GEL-based composite hydrogels for their suitability for 3D bioprinting of C2C12 skeletal muscle cells. The bioinks incorporated various calcium-silicate and zinc-doped MBGNs as BIF. MBGNs of the following compositions were used: $80SiO_2$–20CaO, $80SiO_2$–18CaO-2ZnO, $80SiO_2$–15CaO-5ZnO and $80SiO_2$–10CaO-10ZnO (mol%). Five bioink formulations resulted: ADA-GEL, ADA-GEL-8020, ADA-GEL-2Zn, ADA-GEL-5Zn and ADA-GEL-10Zn. Bioprinting parameters, including nozzle dimensions and extrusion pressure, were optimized to minimize shear stress and preserve cell viability. Mitochondrial activity assessed via WST-8 assay over 1, 3, and 7 days revealed enhanced metabolic activity in BIF-containing bioinks compared to pure ADA-GEL, with ADA-GEL-5Zn showing the highest absorbance. Live/Dead and cytoskeletal staining

(Fig. 8) confirmed good cell distribution and viability across all formulations. Notably, cells displayed greater elongation and alignment in the BIF-containing constructs, particularly in ADA-GEL-8020 and ADA-GEL-2Zn, suggesting that BIF incorporation promotes cytoskeletal organization and orientation along the printing direction [106].

Cell alignment improvements were attributed to both the shear-induced orientation during extrusion and potential ionic interactions, particularly from calcium and zinc ions released from the MBGNs [107]. Although the exact contribution of each ion type remained unclear due to their low relative concentrations, the presence of dopants like Zn was associated with enhanced cell behavior without inducing cytotoxic effects, indicating that ion-releasing nanoparticles are promising to enhance the cellular response in such bioprinted structures intended for applications in muscle TE.

Another study highlighting the antibacterial potential of zinc in bone tissue engineering bioprinted scaffolds is the recent work of Loukelis et al [108], who developed an extrusion-based bioink composed of gellan gum (GG) and poly(vinyl alcohol) (PVA) incorporating zinc-doped BG microparticles (ICIE16 composition: 49.46% SiO_2, 33.27% CaO, 1.07% P_2O_5, 6.6% K_2O, 6.6% Na_2O, 3% ZnO; mol.%). The addition of 2.5% w/v Zn-BG microparticles improved printing accuracy while maintaining favorable rheological behavior, suitable for stable multilayer extrusion (Figs. 9a, b). Adipose-derived stromal cells (ADSCs) were homogeneously incorporated into the ink at a concentration of 5×10^6 cells/mL prior to printing. In vitro, Zn-BG showed a mild antibacterial effect, reducing *S. aureus* viability by ~11–13% within 6–24 h and a delayed response against *E. coli* after 48 h, consistent with differences in Gram-positive and Gram-negative cell wall resistance. Zn-BG also enhanced osteogenic and chondrogenic differentiation of ADSCs, evidenced by increased ALP activity (days 7 and 14) and the formation of a dense aggrecan (ACAN) network by day 56 (Figs. 9c, d). In vivo implantation of the 3D-bioprinted constructs in C57BL/6 mice further confirmed their excellent biocompatibility: neither Zn-BG nor control scaffolds induced inflammation, foreign-body response, macrophage fusion, or fibrous encapsulation after 14 days. These outcomes are consistent with the established non-immunogenicity of PVA and the favorable tissue response to GG hydrogels. Moreover, the immunomodulatory role of BG, especially Zn-doped compositions, supported osteochondral regeneration by upregulating anti-inflammatory cytokines and downregulating pro-inflammatory mediators such as TNF-α and IL-1β.

In light-based bioprinting (LBB), light is used to solidify photosensitive hydrogels into 3D structures [109]. These hydrogel bioinks provide both mechanical support and a favorable environment for cell growth, which is the reason why the choice of LBB is so appealing. In a recent work of Sánchez-Rodríguez et al [110], a cost-effective laser-based printer was used to fabricate GelMA scaffolds with and without MBGNs in order to evaluate the method resolution, print fidelity and

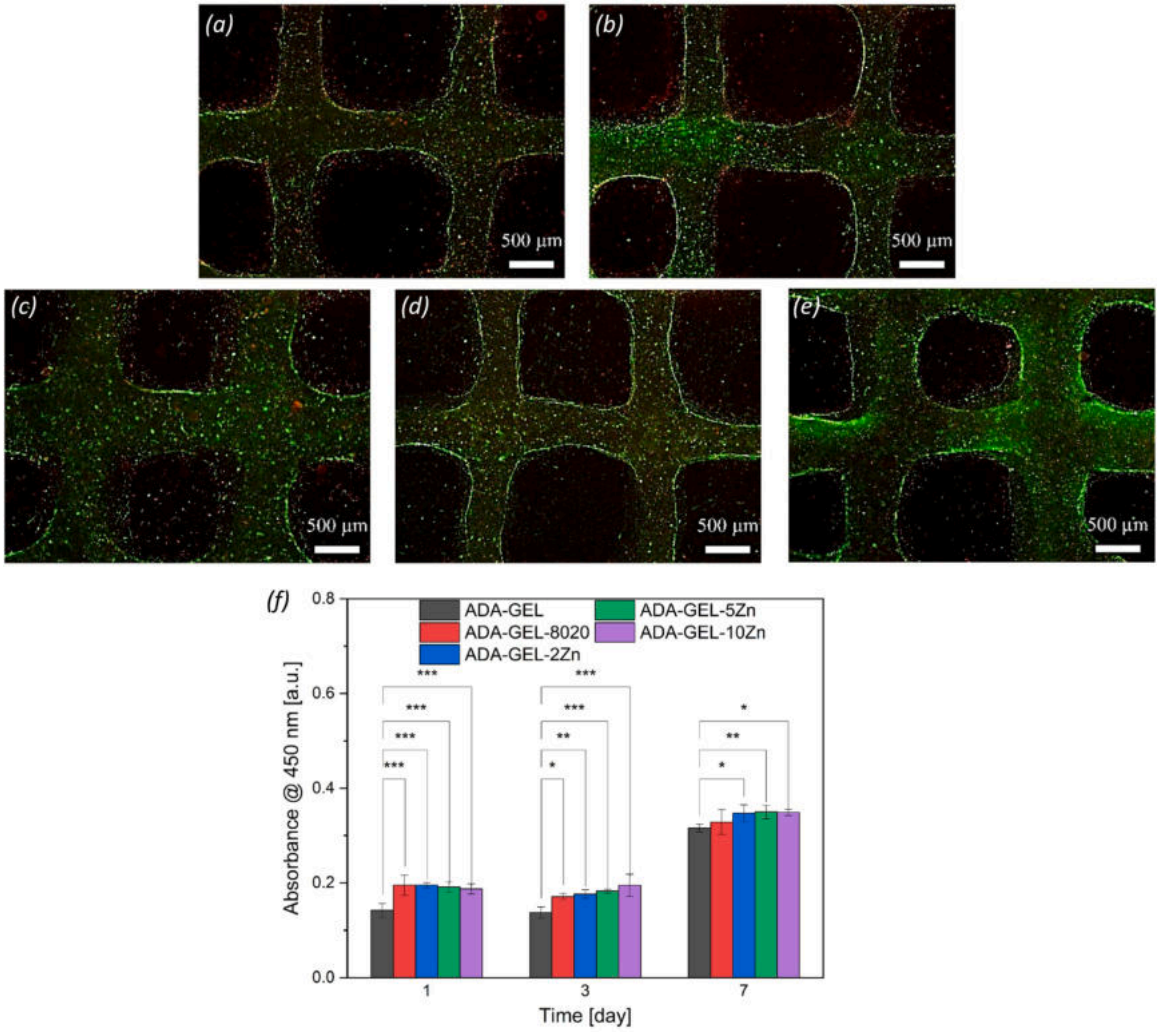

Fig. 8. Results on ADA-GEL/Zn-containing BIF bioinks. Live/Dead staining of bioprinted C2C12 cells after 7 days in (a) ADA-GEL, (b–e) ADA-GEL with increasing Zn- or 8020-BIF content (all scale bars correspond to 500 µm); (f) cell proliferation assessed by WST-8 assay over 7 days. Green = live cells; red = dead cells. Reproduced from Ref.[105] under the terms of the Creative Commons CC-BY license.

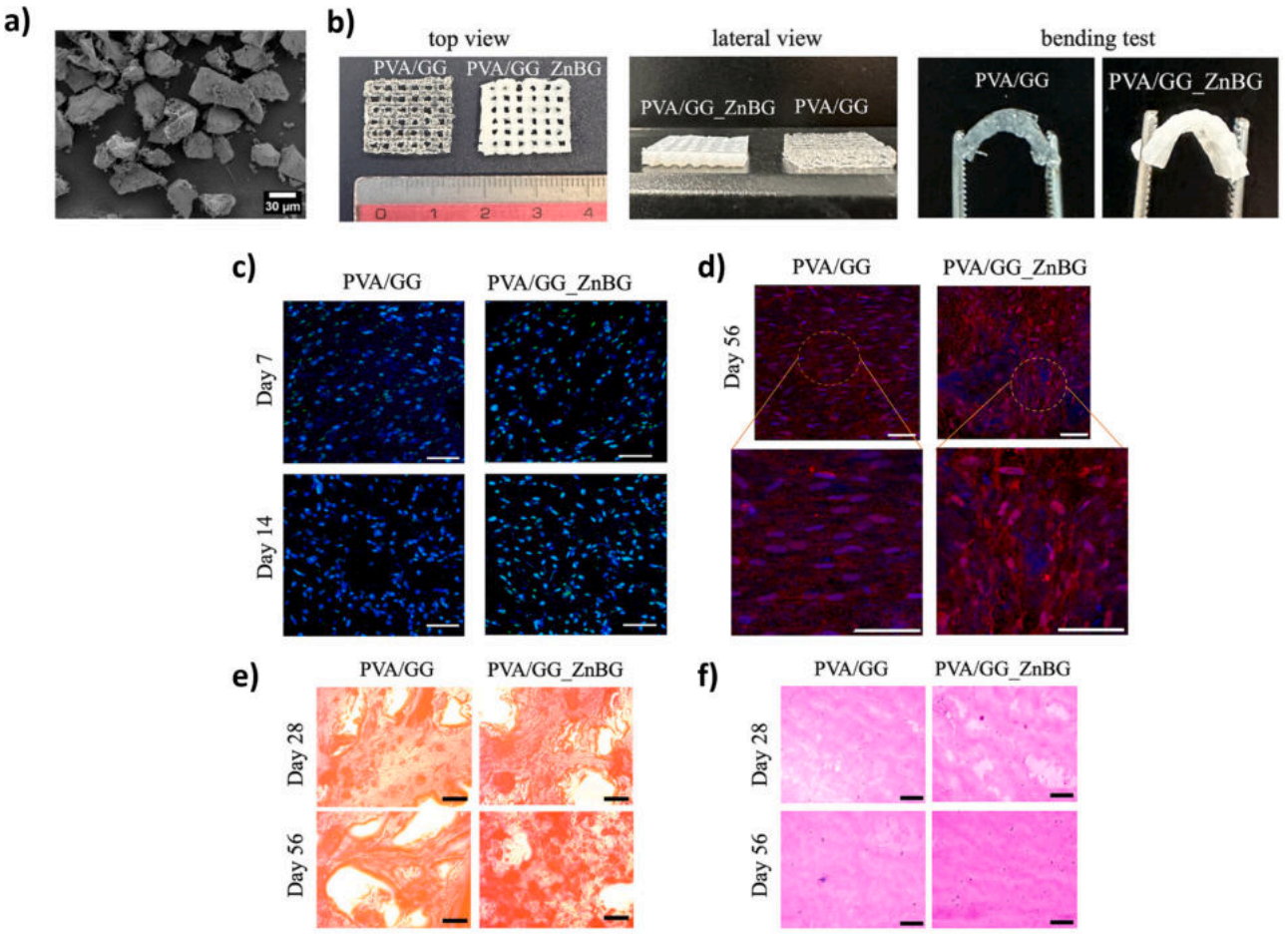

Fig. 9. Results on PVA-GG/Zn-BG containing scaffolds: a) SEM of 3Zn-BG particles (scale bar 30 μm); b) macroscopic top and lateral images of 3D bioprinted constructs and bending test; c) confocal images showing ALP (green) and cell nuclei (blue) after 7 and 14 days (scale bars 100 μm); d) ACAN (red) and cell nuclei (blue) after 56 days with zoomed regions (scale bars 100 μm); e) Sirius Red–stained collagen after 28 and 56 days (scale bars 100 μm); f) glycosaminoglycan formation assessed via DMMB (scale bars 100 μm). Adapted from Ref.[108] with permission from Wiley-VCH GmbH.

suitability for musculoskeletal microtissues. Optical microscopy revealed the formation of thin hydrogel membranes in GelMA-MBGN constructs, likely influenced by the refractive properties of the nanoparticles. Although unintended, these membranes sustained the culture of C2C12 myoblasts, which showed improved proliferation, particularly at the scaffold edges. Notably, C2C12 cells attached and spread within 12 hours post-printing in both pristine GelMA and GelMA-MBGN constructs, a faster response compared with conventional extrusion or inkjet strategies. Fluorescence staining confirmed cell elongation, multinucleation and alignment in both groups, with higher cell density observed in GelMA-MBGN scaffolds (Fig. 10). This enhancement was attributed to the release of silicon and calcium ions from the MBGNs, which promoted cellular metabolism and myogenic differentiation [111], indicating the potential of MBGN-modified GelMA bioinks for muscle TE applications (Fig. 10).

4.2. Bioprinting with borate BGs

Borate-based BGs, which are typically characterized by a more rapid ion release and conversion to HA in physiological conditions with respect to their silicate counterparts [112], can be incorporated into printable polymer matrices to create scaffolds with controlled degradation rates and ion delivery [111,113]. To the best of our knowledge, the fabrication of hydrogel/bioactive borate glass composite scaffolds using 3D bioprinting technology has been investigated by only one research group, integrating adipose-derived stem cells within the hydrogel/BG construct to evaluate cellular viability, osteogenic properties and pro-angiogenic potential. Specifically, borate-based BG microparticles (13-93B3, composition: 53%B_2O_3-20%CaO-12%K_2O-6%Na_2O-5%MgO-4%P_2O_5 (wt.%); particle size <20 μm (d_{50} ~3 μm)) were incorporated in alginate–gelatin (AG) hydrogels for producing bioinks containing human ASCs [60,114]. The hydrogel was formulated by first dissolving 3% w/v gelatin in DMEM at 40°C under stirring, followed by addition of 3% w/v sodium alginate. The BG microparticles were incorporated into the gelatin solution prior to alginate addition at concentrations of 0.075%, 0.15%, 0.3%, and 0.6% w/v, corresponding to 1.25%, 2.5%, 5%, and 10% of the total polymer weight, referred to as 1.25G, 2.5G, 5G, and 10G, respectively. ASCs (1×10^6 cells/mL) were encapsulated in the bioink and printed into six-layered, $15\times15\times1$ mm^3 scaffolds. A critical objective of this work was to assess the cytocompatibility of borate glass microparticles within the 3D constructs, given the fast dissolution kinetics and the risk of borate BGs to release potentially cytotoxic concentrations of ions [115]. In the bioprinted constructs, lattice-like AG, 1.25G, and 2.5G scaffolds were fabricated and cultured for 7 days under dynamic conditions. Live/dead staining (Fig. 11) confirmed high ASC viability in all constructs, although a slightly elevated number of dead cells was observed at scaffold pore edges, likely due to calcium chloride crosslinking. Importantly, while AG scaffolds initially showed a higher viability than 2.5G constructs, this difference was not statistically significant by day 7, indicating that low concentrations of borate BG particles (1.25–2.5%) can be used without eliciting long-term adverse effects on cell survival.

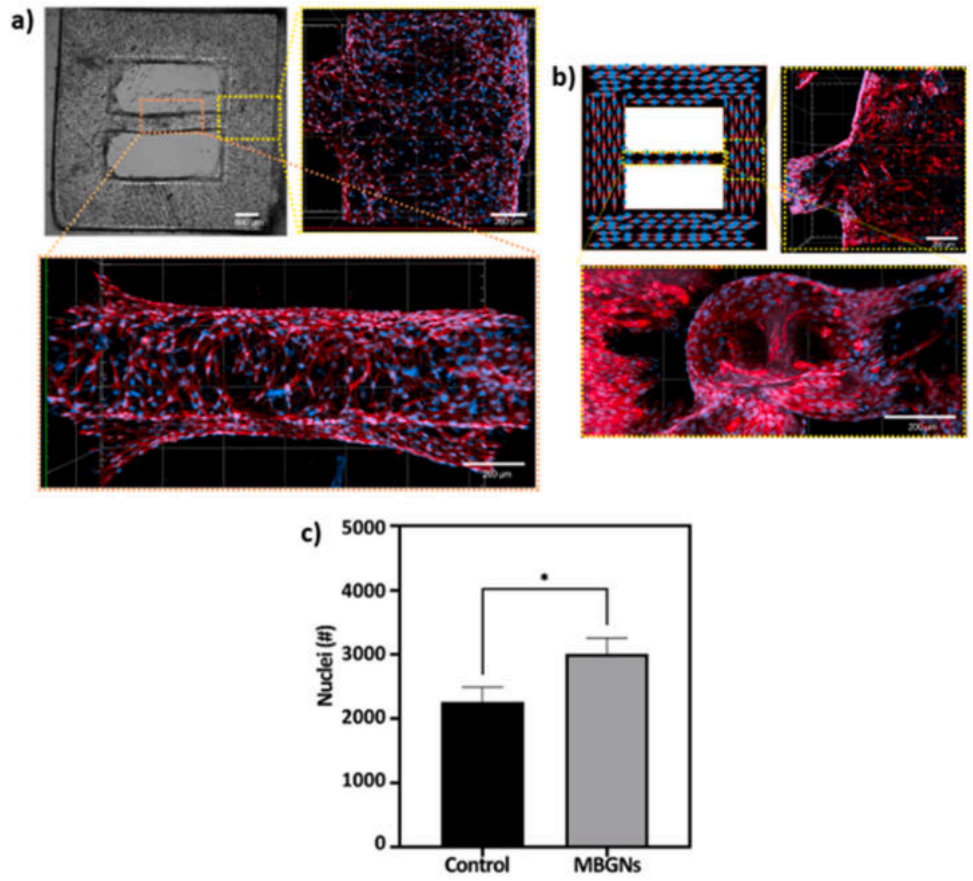

Fig. 10. Results on GelMA-based constructs (control and enriched with MBGNs): (a) images of bright-field microscopy of MBGNs-enriched GelMA construct after 15 days of culture (scale bars from top left to bottom: 500 μm, 200 μm, 200 μm); (b) bright-field image and fluorescence detail showing the deformation of a skeletal muscle GelMA-based construct (not added with MBGNs) after 15 days of culture (scale bars from top to bottom: 200 μm, 200 μm); (c) nuclei counting in GelMA-based constructs loaded with musculoskeletal cells without MBGNs (black bar) and with MBGNs (gray bar) after 20 days of culture. Reproduced from Ref.[110] under the Creative Commons Attribution (CC BY 4.0) license (AccScience Publishing).

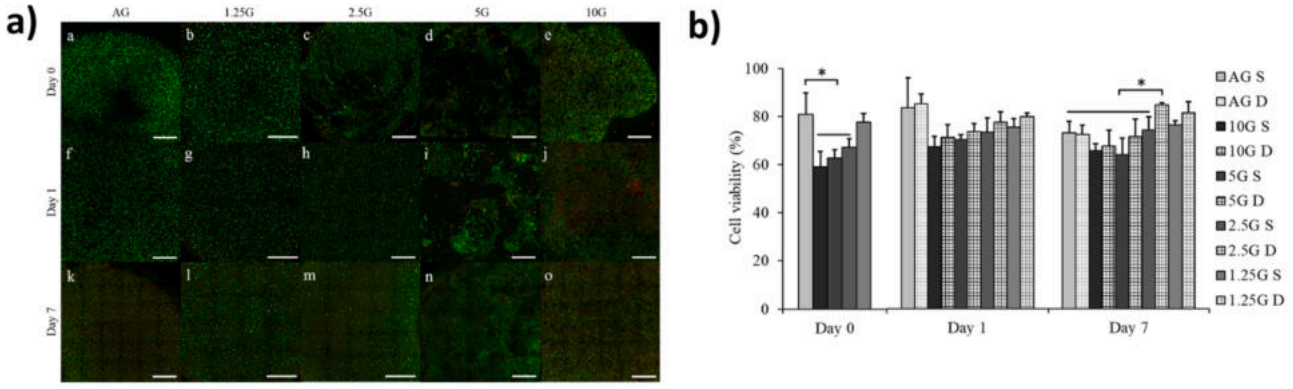

Fig. 11. a) Live/dead assay images of bioprinted AG, 1.25G, and 2.5G scaffolds cultured in dynamic conditions for up to 7 days (all scale bars correspond to 1 mm); b) ASCs viability in AG, 1.25G, and 2.5G bioprinted scaffolds cultured in dynamic condition. Reproduced from Ref.[60] with permission from AccScience Publishing under the Creative Commons Attribution (CC BY 4.0) license.

Overall, the results of the studies [60,114,115] highlighted the potential of borate-based BGs in micro-particulate form to act as a functional additive for AG hydrogels for 3D bioprinting of stem-cell-laden constructs. However, the application of borate-containig BGs is highly concentration-dependent, with low levels (<0.15% w/v) supporting ASC viability and higher concentrations (>0.3% w/v) resulting in cytotoxicity due to pH shifts and ionic imbalance.

4.3. *Bioprinting with phosphosilicate BGs*

Phosphosilicate BGs (PSBGs), containing SiO_2, CaO, and P_2O_5, are known for their ability to form a HA layer under physiological conditions [116–118]. According to the literature, the inclusion of small amounts of phosphorus (up to 5 mol.%) in silicate-based BGs can enhance the glass reactivity and accelerate HA formation [119] on the surface when in contact with biological fluids. The use of silicate MBGs

containing small amounts of P_2O_5 (<5 mol.%) for bioprinting has been reviewed in section 4.1 already; however, only one study [120] has reported the use of phosphosilicate glasses with high content of P_2O_5 in 3D bioprinting, highlighting a significant gap in research in this specific field. In this study [120], PSBG particles (10.8%P_2O_5–54.2%SiO_2–35.0% CaO, mol%) in micrometric size (<30 μm) [121,122] were incorporated into alginate/gelatin-methacrylate (Alg/GM) hydrogels to create bioinks for 3D bioprinting of full-thickness skin substitutes. The Alg/GM hydrogels were prepared using 0–5 wt.% sodium alginate and GelMA dissolved in 0.9% saline. PSBG powder was added at concentrations of 0, 1, 5, and 10 mg/mL. For bioprinting, two bioinks were used: 2Alg15Gel as the epidermis layer, and 2Alg3GM with or without incorporated glass as the dermis, each loaded with HUVECs and MSCs at 2×10^6 and 1×10^6 cells/mL, respectively. The dermal bioink was printed at 10°C, and the epidermal bioink at 37°C. Constructs were printed forming 10-layered cylindrical skin substitutes (15 mm diameter). CD31 immunostaining on day 1 (Fig. 12) showed that 5 mg/mL PSBG particles significantly enhanced CD31 expression and promoted endothelial cell migration. qPCR and in vivo analyses demonstrated that adding 5 mg/mL PSBGs enhanced angiogenesis, promoted M2 macrophage polarization, collagen remodeling and neovascularization, confirming the high potential of incorporating PSBGs into printable cell-laden hydrogels for skin TE through 3D bioprinting.

5. Discussion

Integrating BGs in bioinks for 3D bioprinting is an auspicious strategy for TE and for developing 3D testbeds for investigating the effect of biologically active ions on cellular response. BGs are known for their outstanding properties, like osteoconductivity, osteoinductivity, proangiogenic, antibacterial and immunomodulatory effects. However, when inserting BGs (usually in particulate form) in cell-laden bioinks, there are several challenges regarding printability and mechanical properties that must be further investigated [37]. Analyzing the literature, it becomes clear that there is a paucity of studies about this very specific topic (a summary of key available publications is presented in Table 1) and future research will be required to generate more relevant data that will enable designing advanced 3D bioprinting strategies incorporating BG micro- and nanoparticles into printable hydrogels.

From a methodological viewpoint, it cannot be ignored that a systematic and reliable comparison among the studies collected in Table 1 is not possible due to the lack of standardized experimental conditions: in fact, there is a quite broad variability in terms of BG compositions, BG particle size distribution (which is in turn associated to the method of BG production), hydrogel matrix (i.e., the chemical composition and nature of the polymeric component(s)), BG concentration in the bioink, scaffold geometry and size, and type of cells used, just to name a few parameters of interest. In addition, the complexity of this scenario is increased by the fact that a single parameter can be related to multiple effects relevant to both printing technology and functional properties of the bioinks; for example, BG particle size plays a role in bioink viscosity/printability as well as on BG dissolution/ion release kinetics and biological effects on cells. Nevertheless, some general indications and suggestions can be proposed to stimulate discussion and further research, as discussed next.

5.1. Concentration and compositional limits

The concentration of particulate silicate BGs incorporated in bioinks varies in the range of 0.1 to 10 wt.% [63], while borate-based compositions usually require a much narrower therapeutic window (0.3 wt.%) [60]. Indeed, such a relatively low percentage of rigid bioactive inclusions is desired for allowing adequate printability of the ink and a homogenous dispersion of the particles in the hydrogel, as well as for minimizing possible physico-mechanical damage to living cells associated with their contact with the surface of the glass particles. Despite these low weight fractions, the addition of BG particles, particularly nanoparticles in mesoporous form, significantly improves the construct's functionality. The high specific surface area and ordered mesoporous architecture of MBGNs serve as reservoirs for therapeutic ions and

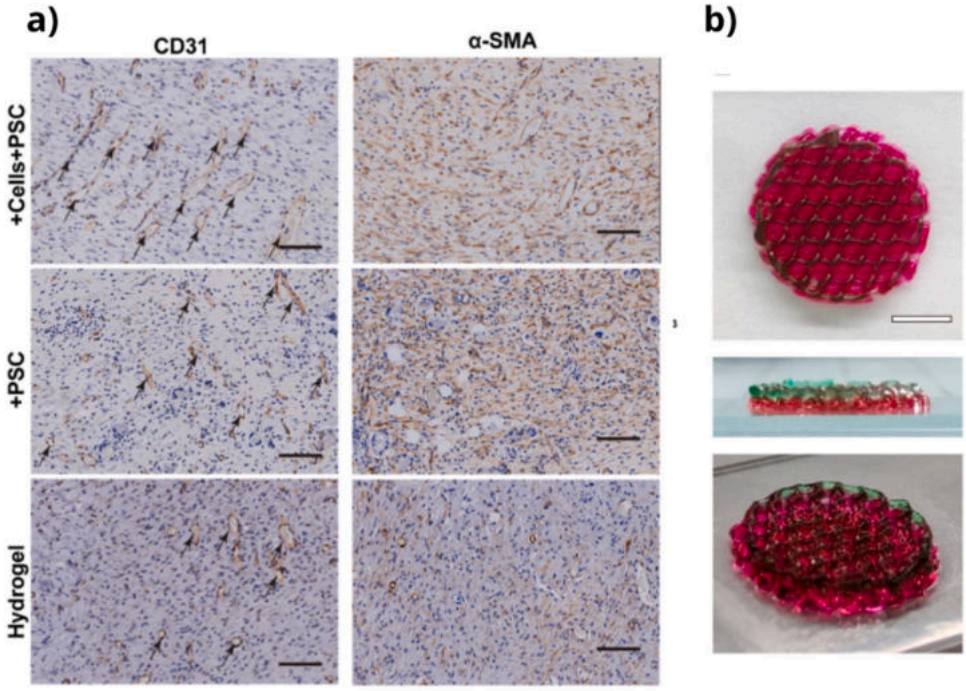

Fig. 12. Histomorphological evaluation of angiogenesis in wounds. Images of immunohistochemistry staining for (a) CD31 (brown) and α-SMA (brown) of wound beds treated with the printed full-thickness skin substitutes (+ Cells + PSC), the printed 2Alg3GM5PSC hydrogels (+PSC), and the printed 2Alg3GM hydrogels (hydrogel) at day 14 post-surgery (scale bars 100 μm). (b) Image of printed epidermis (red) and dermis (green) layer (scale bars 5 mm). Reproduced from Ref.[120] with permission from Elsevier under a CC BY-NC-ND license.

Table 1
Summary of existing studies about bioprinting with BGs (including also pure silica). In all cases bioprinting was carried out by extrusion methods.

Bioactive glass type	BG particle size	Hydrogel matrix	Cell type	Cell density	Bioprinter type	Size of scaffold	Biological evaluation	Application	Reference, publication year
0.4% and 0.8% (w/v) MSNs loaded with BMP-4	139.7 nm	3% gelatin, 5% GelMA, 2% PEG, 0.2% LAP	BMSCs and macrophages (RAW264.7)	1×10^7 cells/mL (both BMSCs and RAW cells)	Pneumatic extrusion (3D Bioplotter)	-	Live/Dead (24 h), CCK-8, macrophage polarization	Bone defects (rats with diabetes mellitus)	[77], 2021
6 wt.% SiNPs and aminopropyl-modified SiNPs (AmMPs)	37.6-108 nm	3% alginate, 3.5% gellan (w/v)	Bovine chondrocytes isolated from bovine knee articular cartilage	1×10^8 cells/mL	Pneumatic extrusion (Cellink INKREDIBLE)	Large-scale construct (cm-scale)	Live/Dead, Col I/II immunostaining	Cartilage	[63], 2018
0.5% MSNCaPDex (MSN functionalized with Ca and P ions and loaded with dexamethasone)	63 ± 8 nm	10% w/v GelMA (0.6 g methacrylic anhydride /g gelatin)	hBM-MSCs	4×10^6 cells/mL	Pneumatic extrusion (Cellink INKREDIBLE+)	Disks (⌀ 20 mm)	Live/Dead, alamarBlue, DNA quant., BMP expression, HA Fluorescence Staining, Alizarin Red Staining	Bone	[90], 2021
3-10% MBGs, (80Si–5P–15Ca/Zn, wt.%)	<45 μm	alginate and methylcellulose blend (3:6%wt and 3:9%wt)	Human mesenchymal stem cells (MSC)	1×10^6 cells/mL	Extrusion (GeSiM BioScaffolder 3.1)	Square shape	DNA quant.	Bone	[98], 2021
0.1% and 0.5% (w/v) BGNPs ($55SiO_2$–$40CaO$–$5P_2O_5$, mol.%), and BGNPsSr ($55SiO_2$–$30CaO$–$5P_2O_5$–10SrO, mol.%)	~30-40 μm	5%w/v ADA and 5%w/v GEL	Osteoblast-like MG-63 cells	-	Extrusion (GeSiM BioScaffolder 2.1)	Square shape (7.75×7.75 mm)	Live/Dead, cell counting	Bone	[95], 2016
BGNPs (66Si–27Ca–7P mol.%)	55 nm	alginate and gelatin blend	Human osteogenic sarcoma cells (SaOS-2)	-	Extrusion (3D-Bioplotter, Envisiontec)	Disks (⌀ 13 mm)	MTT cell viability assay, Alizarin Red Staining,	Bone	[99], 2014
10 wt.% MBG ($80SiO_2$-$15CaO$-$5P_2O_5$, mol%) loaded with DOX	-	5% GelMA, 1% HAMA, 0.5% LAP (w/v)	Murine mesenchymal stem cells (C3H10T1/2)	1×10^7 cells/mL	Extrusion (3D-Bioplotter, Envisiontec)	-	CCK-8 assay, ALP Activity, Alizarin Red Staining	Bone	[101], 2021
5%(w/v) BG microspheres ($60SiO_2$–$36CaO$–$4P_2O_5$)	-	15% GelMA, 10% soldium alginate, 0.5% photoinitiator (w/v)	BMSCs	1×10^7 cells/mL	Extrusion (Bio-Architect ®WS)	(10 × 10 × 5 mm)	Live/Dead, CCK-8 assay, ALP activity, Alizarin Red Staining, expression of osteogenesis-related genes, in vivo (beagles)	Periodontal tissue	[32], 2023
0.1% bioactive inorganic filler ($80SiO_2$–$20CaO$, mol %)	150-400 nm	2,5% ADA-3.75% GEL	NIH/3T3 fibroblasts	1×10^6 cells/mL	Extrusion (BioX printer CellInk)	Grid structure (15 × 15 mm)	Live/Dead, Phalloidin/ DAPI Staining	Soft TE	[104], 2022
0.1% MBGN ($80SiO_2$–$20CaO$, $80SiO_2$–$18CaO$-$2ZnO$, $80SiO_2$–$15CaO$-$5ZnO$, $80SiO_2$–$10CaO$-$10ZnO$, mol %)	110-184 nm	2.5%ADA-3.75% GEL	Skeletal muscle C2C12 cells	2×10^6 cells/mL	Extrusion (BioX printer CellInk)	Grid structure (15 × 15 × 1 mm)	Live/Dead, Phalloidin/ DAPI Staining	Skeletal muscle tissues	[105], 2025

(*continued on next page*)

Table 1 (*continued*)

Bioactive glass type	BG particle size	Hydrogel matrix	Cell type	Cell density	Bioprinter type	Size of scaffold	Biological evaluation	Application	Reference, publication year
2.5% and 3% (w/v) BG (49.46SiO_2-33.27CaO-1.07P_2O_5-6.6K_2O-6.6Na_2O-3ZnO, mol%)	<38 μm	10% PVA, 4% gellan gum (w/v)	ASCs	5×10^6 cells/mL	Pneumatic extrusion (Cellink INKREDIBLE+)	Grid structure (⌀ 1.4 cm x 0.2 cm^3)	Cell viability, ALP activity, Aggrecan visualization, Real Time PCR, histology (H&E), in vivo (C57BL/6 mice)	Osteochondral tissue	[108], 2026
0.5% MBGNs (70SiO_2–30CaO mol.%)	159 ± 29 nm	GelMA	Skeletal muscle C2C12 cells	4×10^6 cells/mL	LBB (Anycubic Photon Mono 4K 3D printer cutomized)	3.6 mm × 3.6 mm × 0.8 mm	Live/Dead, Phalloidin/DAPI staining	Skeletal muscle tissues	[110], 2024
0.075, 0.15, 0.3, 0.6% (w/v) 13-93B3 glass (53B_2O_3–20CaO–12K_2O–6Na_2O–5MgO–4P_2O_5 wt.%)	<20 μm	3%Alginate-3% Gelatin	ASCs	1×10^6 cells/mL	Extrusion based custom-modified cartesian 3D printer	Grid structure (15 × 15 × 1 mm3)	Live/Dead	Bone	[60], 2024
0.075 and 1wt.% PSBG (10.8P_2O_5–54.2SiO_2–35.0CaO mol.%)	-	2%Alginate - 15% Gelatin, Alginate-GelMA	HUVECs, MSCs	2×10^6cells/mL (HUVECs) 1×10^6 cells/mL (MSCs)	Extrusion (SIA PRO)	Cylindrical construct of 15 mm in diameter, with ten layers in height	Live/Dead, Q-PCR, Phalloidin/DAPI Staining, Immunofluorescence, histology (H&E), Immunohistochemistry, Masson's trichrome Staining, in vivo	Skin	[120], 2024

biomolecules, which can be released locally to effectively interact with cells. Beyond drug loading, these nanoparticles act as critical rheological modifiers; their surface charge and nanosize enable the formation of multifunctional electrostatic networks within the bioink, significantly enhancing shear-thinning behavior and the structural fidelity of the printed construct [123].

However, the binding capacity that makes BGs ideal for drug delivery also can create a paradox during in vitro validation. It was observed that BGs can function as 'fluorescent sinks', non-specifically adsorbing common assay reagents, such as calcein and cellular components released after lysis. This sequestration can lead to the misinterpretation of cell viability and differentiation data, as the nanoparticles may mask or mimic vital cellular signals [124]. While the studies reported in Table 1 did not exhibit any apparent cytotoxicity at the BG concentrations tested, this analytical interference suggests that assessing cytotoxicity limits and thresholds deserves more in-depth, dedicated, and standardized studies in the future.

5.2. Ion signaling and therapeutic bioactivity

It is well known that cells can “sense” the presence of biologically active ions released from BGs into the extracellular environment [125], especially if the glass particles are produced in a highly reactive mesoporous nanometric form, having an ultrahigh specific surface area that accelerates their dissolution kinetics. Consequently, the incorporation of ion-releasing BG (nano)particles into printable hydrogels offers a very convenient approach to investigate accurately (in 3D) the biological effects of such ions on a variety of cell types. The release of ionic dissolution products from BG nanoparticles, like calcium, silicate and phosphate ions, is responsible for the main biological effects when BGs are used in bioinks. The cellular activity is affected by the concentration of such ions leading to stimulation of osteogenesis/angiogenesis, immunomodulation and other cellular effects [126,127]. In addition, BG particles can be designed and fabricated with multiple compositions, i.e. doped with biologically active metallic ions, which can be released inside the bioink to have specific effects on the laden cells [128]. In this regard, ionic medicine and particularly ion-assisted tissue regeneration strategies are emerging as promising and fascinating approaches in the field of tissue engineering, offering a potentially simpler and more affordable alternative to conventional drug- or biomolecule (growth factor)-based therapies. In addition, ion release can be an effective (antibiotic drug free) antimicrobial approach to tackle the problem of bacterial resistance, which is correlated to the extensive use of antibiotics.

When BGs incorporated in bioinks are synthesized in a mesoporous form, a synergistic therapeutic mechanism can be exploited via the simultaneous release of (i) biologically active ions as the material dissolves and (ii) drugs or growth factors incorporated in the nano-sized pores of MBGs particles [93]. Finding the dosage thresholds (uptake and release) for both ions and biomolecules in order to ensure a sustained and ideally synergistic therapeutic effect is one of the grand challenges of MBG-based tissue engineering strategies, which indeed must be considered also in the field of bioprinting with BGs.

5.3. Bioink rheology and printability

In general, the mechanical, rheological and biological properties of cell-laden 3D-printed scaffolds are highly impacted by the addition of BG particles. One challenge is that their addition often increases viscosity and bioink heterogeneity, which can compromise printability, reduce extrusion consistency, and lead to excessive stiffening [123,129]. At the same time, it has been frequently reported that the higher viscosity, although requiring greater pressure and slower printing speeds, provides an improved shape fidelity [124]. While the diversity in particle sizes and BG types complicates the identification of a single optimal concentration, a loading of 1-5 w/v% is generally effective for enhancing shear-thinning. However, using a lower threshold of <1 w/v % is often preferred to ensure smooth extrusion without clogging and to protect cell integrity by minimizing the shear stress generated during extrusion. Thus, although the addition of BG particles alters the rheological profile of bioinks, the resulting shear-thinning behavior is actually beneficial for extrusion-based bioprinting [130,131]. In this context, nanosilicates such as halloysite deserve to be mentioned, as their unique “house-of-cards” structure can further improve printability [63].

When designing BG-containing bioinks, volume fraction is a more appropriate metric than weight concentration, since sol–gel-derived MBGs have a lower density and therefore occupy a larger volume at equal mass compared to melt-derived BGs. Particle size and their shape also play a critical role: while direct studies on BG microparticles are limited, nanosized inorganic fillers in general have been shown to reinforce bioink mechanical properties [132,133] avoiding or minimizing the risk of nozzle clogging in extrusion-based processes. Extensive work has been carried out using nanosilicates as nanofillers in extrusion-based bioprinting, demonstrating how nanoscale inorganic phases can modulate rheology and printability. For example, Chimene et al [134] reported that nanosilicates form weak, reversible electrostatic interactions with GelMA and κ-carrageenan, generating a dynamic network that imparts pronounced shear-thinning behavior and rapid viscosity recovery, two essential features for smooth extrusion and shape fidelity. Similarly, other study [135] has shown that incorporating nanosilicates at concentrations around 6 wt% can increase the compressive modulus by approximately 2.5-fold, achieving stiffness levels comparable to those of load-bearing tissues such as cartilage. The size of inorganic fillers has also a functional effect on the ionic release kinetics and, thus, on cellular signaling pathways activated by ionic dissolution products. Clearly, the smaller the particle size, the larger the specific surface area, the faster the BG solubility and ultimately the ion release kinetics.

5.4. Biological performance and challenges for clinical translation

Printing cells directly in the “optimal” ink has undeniable advantages as compared to post-printing cell seeding onto scaffolds, including the shortage of implant fabrication time, more homogeneous distribution of cells throughout the volume of the implantable construct, as well as lower cost and use of resources [136]. In addition, extrusion-based bioprinting has the capacity to deposit high cell densities, reaching physiological levels, thereby enhancing the functional relevance of the target tissue. With regard to the key aspects of bioink printability and cell survival during the printing process, BG particle size and surface chemistry should be controlled for uniform dispersion and smooth extrusion without compromising cell viability. Furthermore, the concentration of BG particles within the bioink must be carefully tuned to achieve a fine balance between mechanical integrity and favorable cellular responses.

Regarding the type of cells to be incorporated in the bioink, it should be consistent with the target tissue to be regenerated. As shown in Table 1, stem cells or immortalized cell lines have been typically incorporated in BG containing bioinks instead of primary cells that, although being immediately able to produce newly-formed tissue, are more delicate with a restricted proliferation rate compared to the other options. Moving from resilient cell lines to the use of patient-specific primary cells within bioactive inks, remains one of the most significant challenges for the clinical translation of this technology.

Recent reviews [128,137] have considered the different mechanisms by which silica and BG nanoparticles can be internalized by cells and have described the fate of the (bioreactive) nanoparticles upon cell internalization. Smaller BG particles (e.g. MBGNs) are easier for cells to detect and internalize; however, further research is needed to determine if there is an optimum size threshold [91,137]. Importantly, while ion release from MBGs is beneficial for triggering biological responses,

excessive concentrations can be detrimental. Therefore, the particle loading within the hydrogel must be carefully optimized to avoid cytotoxic effects. For instance, Kolan et al [60] demonstrated that borate-based BG particles become toxic when they are incorporated above 0.3 wt% in hydrogel formulations. Finally, a major challenge in bioprinting remains minimizing cell damage during the entire fabrication pipeline (bioink preparation, extrusion process, hydrogel crosslinking) while maintaining satisfactory cell viability, appropriate cell phenotype, and desired cell functions in the post-printing culture environment in vitro or, even more crucially, after in vivo implantation.

6. Conclusions and future perspectives

The emerging field of 3D bioprinting with bioinks incorporating BG particulate is a very promising approach in regenerative medicine as revealed by the research works reviewed in this paper. However, there are still numerous aspects that remain to be investigated. At present, almost all the research in this specific field is focused on silicate BG particles, including MBGNs, with very little attention paid to other glass systems like borate or phosphate compositions. Having more insight on how such bioreactive ion-releasing BGs can behave in bioinks will help obtain not only improved bioprinting results but also better post-printing scaffold performance. As this cross-study analysis demonstrates, the search for an optimal bioink transcends glass chemistry and requires a “synchronization” between the volumetric occupancy of the particles, the controlled ion-release kinetics from the BG and the mechanical resilience of the chosen cell type.

The studies reviewed here collectively highlight the growing potential of integrating BG particles into printable hydrogels to enhance both the biological and mechanical performance of bioprinted constructs. From silica-based systems, which enhance print fidelity and osteoinduction, to borate and phosphosilicate BGs that accelerate degradation and ion release, BGs offer remarkable versatility in tailoring scaffold functionalities. Their incorporation in hydrogels improves rheological properties and ion-mediated cell signaling, without compromising cell viability in most systems with controlled BG concentrations. In addition to specific tissue-targeted approaches, bioinks incorporating ion-releasing BG particles can be exploited to generate precise testbeds (3D in vitro systems) to enable the study of biologically active ion-cell interactions in 3D. Moreover, beyond conventional extrusion approaches, emerging techniques such as multimaterial chaotic printing enable the spatial organization of BG-containing phases within hydrogels, creating microarchitectured constructs that resemble the natural complexity of tissue environments [37,138].

Despite encouraging in vitro and in vivo findings, particularly in bone regeneration, systematic investigations remain limited. Direct comparisons between bioprinted and cell-laden constructs using standardized architectures, identical cell types and consistent material formulations are still lacking in the literature. Overall, the integration of BGs into bioinks represents a promising strategy to bridge material functionality with biological performance in the next generation of tissue-engineered constructs.

CRediT authorship contribution statement

Maria Erato Pianou: Writing – original draft, Investigation, Conceptualization. **Andreea Luiza Mîrț:** Writing – original draft, Investigation, Conceptualization. **Valentina Rigano:** Writing – original draft, Investigation, Conceptualization. **Enrica Verné:** Writing – review & editing, Supervision, Investigation, Conceptualization. **Francesco Baino:** Writing – review & editing, Supervision, Project administration, Investigation, Funding acquisition, Conceptualization. **Aldo R. Boccaccini:** Writing – review & editing, Supervision, Investigation, Funding acquisition, Conceptualization.

Declaration of competing interest

The authors declare that they have no known competing financial interests or personal relationships that could have appeared to influence the work reported in this paper.

Acknowledgement

This study was partially carried out within the project “End-to-end multidisciplinary optimal design for improved personalized bioactive glass/ceramic bone substitute implants” (ReBone) funded by the European Union’s Horizon Europe research and innovation programme under the Grant Agreement no. 101119884. This manuscript reflects only the authors’ views and opinions and the Ministry cannot be considered responsible for them. The work was also partially conducted in the framework of Collaborative Research Center SFB/TRR225 'From the fundamentals of Biofabrication to functional tissue models' – project number 326998133 – TRR 225 (subproject B03), funded by the German Research Foundation (DFG).

References

[1] S.A. Goldstein, M.R. Moalli, Current concepts in tissue engineering: cell, matrices, and genes, Curr. Opin. Orthop. 12 (2001) 424–427, https://doi.org/10.1097/00001433-200110000-00010.
[2] E.S. Place, N.D. Evans, M.M. Stevens, Complexity in biomaterials for tissue engineering, Nat. Mater. 8 (2009) 457–470, https://doi.org/10.1038/nmat2441.
[3] I. Benjumeda Wijnhoven, R. Vallejos, J.F. Santibanez, C. Millán, J.F. Vivanco, Analysis of cell-biomaterial interaction through cellular bridge formation in the interface between hGMSCs and CaP bioceramics, Sci. Rep. 10 (2020) 1–14, https://doi.org/10.1038/s41598-020-73428-y.
[4] B.D. Ratner, A.S. Hoffman, J.E. Lemons, Biomaterials science: an introduction to materials in medicine, 2nd ed., Academic Press, San Diego, 2004.
[5] F.J. O’Brien, Biomaterials & scaffolds for tissue engineering, Mater. Today 14 (2011) 88–95, https://doi.org/10.1016/S1369-7021(11)70058-X.
[6] D.W. Hutmacher, Scaffolds in tissue engineering bone and cartilage, Biomaterials 21 (2000) 175–189, https://doi.org/10.1016/B978-008045154-1.50021-6.
[7] G. Turnbull, J. Clarke, F. Picard, P. Riches, L. Jia, F. Han, B. Li, W. Shu, 3D bioactive composite scaffolds for bone tissue engineering, Bioact. Mater. 3 (2018) 278–314, https://doi.org/10.1016/j.bioactmat.2017.10.001.
[8] A.G. Nandgaonkar, W.E. Krause, L.A. Lucia, Fabrication of Cellulosic Composite Scaffolds for Cartilage Tissue Engineering, Elsevier Ltd, 2016. https://doi.org/10.1016/B978-1-78242-452-9.00009-1.
[9] A.J. Salgado, O.P. Coutinho, R.L. Reis, Bone tissue engineering: State of the art and future trends, Macromol. Biosci. 4 (2004) 743–765, https://doi.org/10.1002/mabi.200400026.
[10] S. Eriksson, L. Sandsjö, Three-dimensional fabrics as medical textiles, 2015. https://doi.org/10.1016/b978-1-78242-214-3.00012-7.
[11] A.J. Steward, Y. Liu, D.R. Wagner, Engineering cell attachments to scaffolds in cartilage tissue engineering, JOM 63 (2011) 74–82, https://doi.org/10.1007/s11837-011-0062-x.
[12] F. Baino, S. Hamzehlou, S. Kargozar, Bioactive glasses: where are we and where are we going? J. Funct. Biomater. 9 (2018) 25, https://doi.org/10.3390/jfb9010025.
[13] S.S. Lee, X. Du, I. Kim, S.J. Ferguson, Review Scaffolds for bone-tissue engineering, Matter 5 (2022) 2722–2759, https://doi.org/10.1016/j.matt.2022.06.003.
[14] Y.H. Kim, S. Vijayavenkataraman, G. Cidonio, Biomaterials and scaffolds for tissue engineering and regenerative medicine, BMC Methods 1 (2024) 2–4, https://doi.org/10.1186/s44330-024-00002-7.
[15] Y. Wang, C. Shangsi, L. Haowen, B. Jiaming, A review of graded scaffolds made by additive manufacturing for tissue engineering: design, fabrication and properties, Biofabrication 17 (2025) 022009, https://doi.org/10.1088/1758-5090/adba8e.
[16] M.M. Germaini, S. Belhabib, S. Guessasma, R. Deterre, P. Corre, P. Weiss, Additive manufacturing of biomaterials for bone tissue engineering – a critical review of the state of the art and new concepts, Prog. Mater. Sci. 130 (2022), https://doi.org/10.1016/j.pmatsci.2022.100963.
[17] C.J. Culbreath, M.S. Taylor, S.D. McCullen, O.T. Mefford, A review of additive manufacturing in tissue engineering and regenerative medicine, Biomed. Mater. Devices 3 (2025) 237–258, https://doi.org/10.1007/s44174-024-00183-3.
[18] H. Qu, Additive manufacturing for bone tissue engineering scaffolds, Mater. Today Commun. 24 (2020) 101024, https://doi.org/10.1016/j.mtcomm.2020.101024.
[19] C. Dong, M. Petrovic, I.J. Davies, Applications of 3D printing in medicine: a review, Ann. 3D Print. Med. 14 (2024) 100149, https://doi.org/10.1016/j.stlm.2024.100149.
[20] J.L. Amaya-Rivas, B.S. Perero, C.G. Helguero, J.L. Hurel, J.M. Peralta, F.A. Flores, J.D. Alvarado, Future trends of additive manufacturing in medical applications:

An overview, Heliyon 10 (2024) e26641. https://doi.org/10.1016/j.heliyon.2024.e26641.
[21] N. Di Marzio, D. Eglin, T. Serra, L. Moroni, Bio-fabrication: convergence of 3D bioprinting and nano-biomaterials in tissue engineering and regenerative medicine, Front. Bioeng. Biotechnol 8 (2020) 326, https://doi.org/10.3389/fbioe.2020.00326.
[22] J. Groll, J.A. Burdick, D. Cho, B. Derby, M. Gelinsky, S.C. Heilshorn, T. Jüngst, J. Malda, A definition of bioinks and their distinction from biomaterial inks, Biofabrication 11 (2019) 013001.
[23] V. Mironov, D. Ph, N. Reis, D. Phil, B. Derby, D. Ph, Bioprinting: a beginning, Tissue Eng. 12 (2006) 631–634, https://doi.org/10.1089/ten.2006.12.631.
[24] S.V. Murphy, A. Atala, 3D bioprinting of tissues and organs, Nat. Biotechnol. 32 (2014) 773–785, https://doi.org/10.1038/nbt.2958.
[25] L.G. Bracaglia, B.T. Smith, E. Watson, N. Arumugasaamy, A.G. Mikos, J.P. Fisher, 3D Printing for the design and fabrication of polymer-based gradient scaffolds, Acta Biomater 56 (2017) 3–13, https://doi.org/10.1016/j.actbio.2017.03.030.
[26] G. Ratheesh, J.R. Venugopal, A. Chinappan, H. Ezhilarasu, A. Sadiq, S. Ramakrishna, 3D fabrication of polymeric scaffolds for regenerative therapy, ACS Biomater. Sci. Eng. 3 (2017) 1175–1194, https://doi.org/10.1021/acsbiomaterials.6b00370.
[27] P. Pitacco, J.M. Sadowska, F.J. O'Brien, D.J. Kelly, 3D bioprinting of cartilaginous templates for large bone defect healing, Acta Biomater. 156 (2023) 61–74, https://doi.org/10.1016/j.actbio.2022.07.037.
[28] A. Schwab, R. Levato, M. D'Este, S. Piluso, D. Eglin, J. Malda, Printability and shape fidelity of bioinks in 3D bioprinting, Chem. Rev. 120 (2020) 11028–11055, https://doi.org/10.1021/acs.chemrev.0c00084.
[29] S.M. Hull, L.G. Brunel, S.C. Heilshorn, 3D bioprinting of cell-laden hydrogels for improved biological functionality, Adv. Mater. 34 (2022) e2103691, https://doi.org/10.1002/adma.202103691.
[30] M.J. Sawkins, P. Mistry, B.N. Brown, K.M. Shakesheff, L.J. Bonassar, J. Yang, Cell and protein compatible 3D bioprinting of mechanically strong constructs for bone repair, Biofabrication 7 (2015), https://doi.org/10.1088/1758-5090/7/3/035004.
[31] R. Rasouli, C. Sweeney, J.P. Frampton, Heterogeneous and composite bioinks for 3d bioprinting of complex tissue, Biomed. Mater. Devices 3 (2025) 108–126, https://doi.org/10.1007/s44174-024-00171-7.
[32] G. Miao, L. Liang, W. Li, C. Ma, Y. Pan, H. Zhao, Q. Zhang, Y. Xiao, X. Yang, 3D bioprinting of a bioactive composite scaffold for cell delivery in periodontal tissue regeneration, Biomolecules 13 (2023), https://doi.org/10.3390/biom13071062.
[33] D. Chimene, K.K.L. Ennox, R.R.K. Aunas, A.K.G. Aharwar, Advanced bioinks for 3d printing: a materials science perspective, Ann. Biomed. Eng. 44 (2016) 2090–2102, https://doi.org/10.1007/s10439-016-1638-y.
[34] E. Zeimaran, S. Pourshahrestani, A. Fathi, N.A. bin A. Razak, N.A. Kadri, A. Sheikhi, F. Baino, Advances in bioactive glass-containing injectable hydrogel biomaterials for tissue regeneration, Acta Biomater. 136 (2021) 1–36, https://doi.org/10.1016/j.actbio.2021.09.034.
[35] D. Chimene, R. Kaunas, A.K. Gaharwar, Hydrogel bioink reinforcement for additive manufacturing: a focused review of emerging strategies, Adv. Mater. 32 (2020) 1902026, https://doi.org/10.1002/adma.201902026.
[36] Y. Cai, S. Yee, S. Wah, S. Ma, W. Feng, C. Yen, Nanocomposite bioinks for 3D bioprinting, Acta Biomater. 151 (2022) 45–69, https://doi.org/10.1016/j.actbio.2022.08.014.
[37] C.F. Ceballos-González, E.J. Bolívar-Monsalve, D.A. Quevedo-Moreno, C. Chávez-Madero, S. Velásquez-Marín, L.L. Lam-Aguilar, Ó.E. Solís-Pérez, A. Cantoral-Sánchez, M. Neher, E. Yzar-García, Y.S. Zhang, C. Gentile, A.R. Boccaccini, M. M. Alvarez, G. Trujillo-de Santiago, Plug-and-play multimaterial chaotic printing /bioprinting to produce radial and axial micropatterns in hydrogel filaments, Adv. Mater. Technol. 8 (2023) 202202208, https://doi.org/10.1002/admt.202202208.
[38] S. Heid, A.R. Boccaccini, Advancing bioinks for 3D bioprinting using reactive fillers: A review, Acta Biomater. 113 (2020) 1–22, https://doi.org/10.1016/j.actbio.2020.06.040.
[39] L.C. Gerhardt, K.L. Widdows, M.M. Erol, C.W. Burch, J.A. Sanz-Herrera, I. Ochoa, R. Stämpfli, I.S. Roqan, S. Gabe, T. Ansari, A.R. Boccaccini, The pro-angiogenic properties of multi-functional bioactive glass composite scaffolds, Biomaterials 32 (2011) 4096–4108, https://doi.org/10.1016/j.biomaterials.2011.02.032.
[40] M.N. Rahaman, D.E. Day, B. Sonny Bal, Q. Fu, S.B. Jung, L.F. Bonewald, A. P. Tomsia, Bioactive glass in tissue engineering, Acta Biomater. 7 (2011) 2355–2373, https://doi.org/10.1016/j.actbio.2011.03.016.
[41] E. Piatti, M. Miola, E. Verné, Tailoring of bioactive glass and glass-ceramics properties for in vitro and in vivo response optimization: a review, Biomater. Sci. 12 (2024) 4546–4589, https://doi.org/10.1039/d3bm01574b.
[42] L.L. Hench, R.J. Splinter, W.C. Allen, T.K. Greenlee, Bonding mechanisms at the interface of ceramic prosthetic materials, J. Biomed. Mater. Res. 5 (1971) 117–141, https://doi.org/10.1002/jbm.820050611.
[43] E. Fiume, J. Barberi, E. Verné, F. Baino, Bioactive glasses: from parent 45s5 composition to scaffold-assisted tissue-healing therapies, J. Funct. Biomater. 9 (2018), https://doi.org/10.3390/jfb9010024.
[44] K. Deshmukh, T. Kovarik, T. Krenek, D. Docheva, T. Stich, J. Pola, Recent advances and future perspectives of sol-gel derived porous bioactive glasses: a review, RSC Adv. 10 (2020) 33782–33835, https://doi.org/10.1039/d0ra04287k.
[45] T.J. Brunner, R.N. Grass, W.J. Stark, Glass and bioglass nanopowders by flame synthesis, Chem. Commun. (2006) 1384–1386, https://doi.org/10.1039/b517501a.
[46] X. Du, D. Wei, L. Huang, M. Zhu, Y. Zhang, Y. Zhu, 3D printing of mesoporous bioactive glass/silk fibroin composite scaffolds for bone tissue engineering, Mater. Sci. Eng. C 103 (2019) 109731, https://doi.org/10.1016/j.msec.2019.05.016.
[47] L. Hench, The story of Bioglass, J. Mater. Sci. Mater. Med. 17 (2006) 967–978, https://doi.org/10.1007/s10856-006-0432-z.
[48] J.R. Jones, Review of bioactive glass: From Hench to hybrids, Acta Biomater. 9 (2013) 4457–4486, https://doi.org/10.1016/j.actbio.2012.08.023.
[49] N. Mutlu, M. Arango-Ospina, R. Detsch, D. Galusek, A.R. Boccaccini, Zinc and gallium doped borate bioactive glasses influence in-vitro angiogenesis: New evidence in cell co-culture studies, Mater. Lett. 377 (2024) 0–4, https://doi.org/10.1016/j.matlet.2024.137529.
[50] M. Lallukka, A. Houaoui, M. Miola, S. Miettinen, J. Massera, E. Verné, In vitro cytocompatibility of antibacterial silver and copper-doped bioactive glasses, Ceram. Int. 49 (2023) 36044–36055, https://doi.org/10.1016/j.ceramint.2023.08.284.
[51] U. Pantulap, M. Arango-Ospina, A.R. Boccaccini, Bioactive glasses incorporating less-common ions to improve biological and physical properties, J. Mater. Sci. Mater. Med. 33 (2022), https://doi.org/10.1007/s10856-021-06626-3.
[52] C. Wu, J. Chang, Multifunctional mesoporous bioactive glasses for effective delivery of therapeutic ions and drug/growth factors, J. Control. Release 193 (2014) 282–295, https://doi.org/10.1016/j.jconrel.2014.04.026.
[53] F. Baino, G. Novajra, V. Miguez-Pacheco, A.R. Boccaccini, C. Vitale-Brovarone, Bioactive glasses: Special applications outside the skeletal system, J. Non-Cryst. Solids 432 (2016) 15–30, https://doi.org/10.1016/j.jnoncrysol.2015.02.015.
[54] V. Miguez-Pacheco, L.L. Hench, A.R. Boccaccini, Bioactive glasses beyond bone and teeth: Emerging applications in contact with soft tissues, Acta Biomater. 13 (2015) 1–15, https://doi.org/10.1016/j.actbio.2014.11.004.
[55] P. Wray, Cotton candy that heals? borate glass nanofibers look promising, Am. Ceram. Soc. Bull. 90 (2011) 25–29.
[56] A.A. Solbu, D. Caballero, S. Damigos, S.C. Kundu, R.L. Reis, Ø. Halaas, A. S. Chahal, B.L. Strand, Assessing cell migration in hydrogels: an overview of relevant materials and methods, Mater. Today Bio. 18 (2023) 100537, https://doi.org/10.1016/j.mtbio.2022.100537.
[57] I. Singh, S.T.R.B. Rao, H.R. Irving, K. Balani, I. Kong, Advanced alginate/58S bioactive glass inks with enhanced printability, mechanical strength, and cytocompatibility for soft tissue engineering, Int. J. Biol. Macromol. 305 (2025) 141106, https://doi.org/10.1016/j.ijbiomac.2025.141106.
[58] Z. Guo, J. Han, Z. Li, Y. Sun, R. Chen, S. ur Rehman, H. Xia, J. Zhang, K. Ma, J. Wang, Borate bioactive glass enhances 3D bioprinting precision and biocompatibility on a sodium alginate platform via Ca2+ controlled self-solidification, Int. J. Biol. Macromol. 277 (2024) 134338, https://doi.org/10.1016/j.ijbiomac.2024.134338.
[59] Q. Huang, Y. Zou, M.C. Arno, S. Chen, T. Wang, J. Gao, A.P. Dove, J. Du, Hydrogel scaffolds for differentiation of adipose-derived stem cells, Chem. Soc. Rev. 46 (2017) 6255–6275, https://doi.org/10.1039/c6cs00052e.
[60] K.C.R. Kolan, A. Saxena, B.A. Bromet, L.B. Steen, A.T. Bindbeutel, J.A. Semon, D. E. Day, M.C. Leu, Bioprinting with adipose stem cells and hydrogel modified with bioactive glass, Int. J. Bioprint. 10 (2024) 458–475, https://doi.org/10.36922/IJB.2057.
[61] A. Iodchik, G. Lusvardi, A. Zambon, P.S. Lee, H.P. Wiesmann, A. Bernhardt, V. Hintze, Gelatin/Cerium-Doped Bioactive Glass Composites for Enhancing Cellular functions of human mesenchymal stem cells (hBMSCs), Gels 11 (2025) 425, https://doi.org/10.3390/gels11060425.
[62] G. Huang, L. Xu, J. Wu, S. Wang, Y. Dong, Gelatin/bioactive glass composite scaffold for promoting the migration and odontogenic differentiation of bone marrow mesenchymal stem cells, Polym. Test. 93 (2021) 106915, https://doi.org/10.1016/j.polymertesting.2020.106915.
[63] M. Lee, K. Bae, P. Guillon, J. Chang, Ø. Arlov, M. Zenobi-Wong, Exploitation of cationic silica nanoparticles for bioprinting of large-scale constructs with high printing fidelity, ACS Appl. Mater. Interfaces 10 (2018) 37820–37828, https://doi.org/10.1021/acsami.8b13166.
[64] E. Fiume, S. Ciavattini, E. Verné, F. Baino, Foam replica method in the manufacturing of bioactive glass scaffolds: Out-of-date technology or still underexploited potential? Materials 14 (2021) 2795, https://doi.org/10.3390/ma14112795.
[65] G. Poologasundarampillai, P.D. Lee, C. Lam, A.M. Kourkouta, J.R. Jones, Compressive strength of bioactive sol–gel glass foam scaffolds, Int. J. Appl. Glass Sci. 7 (2016) 229–237, https://doi.org/10.1111/ijag.12211.
[66] M. Nagrath, A. Alhalawani, A. Rahimnejad Yazdi, M.R. Towler, Bioactive glass fiber fabrication via a combination of sol-gel process with electro-spinning technique, Mater. Sci. Eng. C 101 (2019) 521–538, https://doi.org/10.1016/j.msec.2019.04.003.
[67] C.S. Rodrigo-Vázquez, N. Kamboj, M. Aghayan, A. Sáez, A.H. De Aza, M. A. Rodríguez, I. Hussainova, Manufacturing of silicon – Bioactive glass scaffolds by selective laser melting for bone tissue engineering, Ceram. Int. 46 (2020) 26936–26944, https://doi.org/10.1016/j.ceramint.2020.07.171.
[68] T. Distler, N. Fournier, A. Grünewald, C. Polley, H. Seitz, R. Detsch, A. R. Boccaccini, Polymer-bioactive glass composite filaments for 3d scaffold manufacturing by fused deposition modeling: fabrication and characterization, Front. Bioeng. Biotechnol. 8 (2020) 1–17, https://doi.org/10.3389/fbioe.2020.00552.
[69] M. Navarro, J.A. Planell, Composite scaffolds for bone tissue regeneration, Wiley Encycl. Compos. (2012) 1–14, https://doi.org/10.1002/9781118097298.weoc050.

[70] A. Nommeots-Nomm, P.D. Lee, J.R. Jones, Direct ink writing of highly bioactive glasses, J. Eur. Ceram. Soc. 38 (2018) 837–844, https://doi.org/10.1016/j.jeurceramsoc.2017.08.006.

[71] B. Sarker, D.G. Papageorgiou, R. Silva, T. Zehnder, F. Gul-E-Noor, M. Bertmer, J. Kaschta, K. Chrissafis, R. Detsch, A.R. Boccaccini, Fabrication of alginate-gelatin crosslinked hydrogel microcapsules and evaluation of the microstructure and Physico-chemical properties, J. Mater. Chem. B 2 (2014) 1470–1482, https://doi.org/10.1039/c3tb21509a.

[72] S. Reakasame, D. Trapani, R. Detsch, A.R. Boccaccini, Cell laden alginate-keratin based composite microcapsules containing bioactive glass for tissue engineering applications, J. Mater. Sci. Mater. Med. 29 (2018) 1–7, https://doi.org/10.1007/s10856-018-6195-5.

[73] M. Rahimnejad, C. Charbonneau, Z. He, S. Lerouge, Injectable cell-laden hybrid bioactive scaffold containing bioactive glass microspheres, J. Biomed. Mater. Res. A 111 (2023) 1031–1043, https://doi.org/10.1002/jbm.a.37487.

[74] J.K. Placone, A.J. Engler, Recent advances in extrusion-based 3d printing for biomedical applications, Adv. Healthc. Mater. 7 (2018) e1701161, https://doi.org/10.1002/adhm.201701161.

[75] M.E. Cooke, D.H. Rosenzweig, The rheology of direct and suspended extrusion bioprinting, APL Bioeng. 5 (2021) 011502, https://doi.org/10.1063/5.0031475.

[76] Y. Ji, T. Kim, I. Jang, J.B. Lee, Electrochromic DNA–Based bioink with rapid interfacial gelation for bioprinting applications, Nanoscale Horiz. 10 (2025) 3499–3505, https://doi.org/10.1039/D5NH00488H.

[77] X. Sun, Z. Ma, X. Zhao, W. Jin, C. Zhang, J. Ma, L. Qiang, W. Wang, Q. Deng, H. Yang, J. Zhao, Q. Liang, X. Zhou, T. Li, J. Wang, Three-dimensional bioprinting of multicell-laden scaffolds containing bone morphogenic protein-4 for promoting M2 macrophage polarization and accelerating bone defect repair in diabetes mellitus, Bioact. Mater. 6 (2021) 757–769, https://doi.org/10.1016/j.bioactmat.2020.08.030.

[78] L. Sprenger, H.H. Lu, S. Trippmacher, U. Mansfeld, P. Milkin, L. Ionov, G. Papastavrou, A.R. Boccaccini, S. Salehi, Composite alginate dialdehyde-gelatin (ada-gel) hydrogel containing short ribbon-shaped fillers for skeletal muscle tissue biofabrication, ACS Appl. Mater. Interfaces 16 (2024) 44605–44622, https://doi.org/10.1021/acsami.4c10751.

[79] Z. Yazdanpanah, J.D. Johnston, D.M.L. Cooper, X. Chen, 3D bioprinted scaffolds for bone tissue engineering: state-of-the-art and emerging technologies, Front. Bioeng. Biotechnol. 10 (2022) 824156, https://doi.org/10.3389/fbioe.2022.824156.

[80] K.A. Deo, K.A. Singh, C.W. Peak, D.L. Alge, A.K. Gaharwar, Bioprinting 101: design, fabrication, and evaluation of cell-laden 3d bioprinted scaffolds, Tissue Eng. Part A 26 (2020) 318–338, https://doi.org/10.1089/ten.tea.2019.0298.

[81] S.M. Hull, C.D. Lindsay, L.G. Brunel, D.J. Shiwarski, J.W. Tashman, J.G. Roth, D. Myung, A.W. Feinberg, S.C. Heilshorn, 3D Bioprinting using UNIversal Orthogonal Network (UNION) Bioinks, Adv. Funct. Mater. 31 (2021) 1–11, https://doi.org/10.1002/adfm.202007983.

[82] F. Bider, E. Karakaya, D. Mohn, A.R. Boccaccini, Advantages of nanoscale bioactive glass as inorganic filler in alginate hydrogels for drug delivery and biofabrication, Eur. J. Mater. 2 (2022) 33–53, https://doi.org/10.1080/26889277.2022.2039078.

[83] J. Wilson, G.H. Pigott, F.J. Schoen, L.L. Hench, Toxicology and biocompatibility of bioglasses, J. Biomed. Mater. Res. 5 (1981) 805–817.

[84] I. Izquierdo-Barba, M. Vallet-Regí, Mesoporous bioactive glasses: relevance of their porous structure compared to that of classical bioglasses, Biomed. Glas. (2015) 1, https://doi.org/10.1515/bglass-2015-0014.

[85] K. Czarnobaj, M. Prokopowicz, W. Sawicki, Formulation and In *Vitro* characterization of bioactive mesoporous silica with doxorubicin and metronidazole intended for bone treatment and regeneration, AAPS PharmSciTech 18 (2017) 3163–3171, https://doi.org/10.1208/s12249-017-0804-3.

[86] M. Vallet-Regí, L. Ruiz-González, I. Izquierdo-Barba, J.M. González-Calbet, Revisiting silica based ordered mesoporous materials: Medical applications, J. Mater. Chem. 16 (2006) 26–31, https://doi.org/10.1039/b509744d.

[87] Q. Yao, Y. Liu, B. Selvaratnam, R.T. Koodali, H. Sun, Mesoporous silicate nanoparticles/3d nanofibrous scaffold-mediated dual-drug delivery for bone tissue engineering, J. Control. Release 279 (2018) 69–78, https://doi.org/10.1016/j.jconrel.2018.04.011.

[88] Y. Tian, Z. Li, W. Zhang, Y. Li, Y. Yuan, C. Liu, Size-mediated adsorption dynamics, conformation and bioactivity of bone morphogenetic protein-2 onto silica nanoparticles, J. Nanosci. Nanotechnol. 16 (2016) 5528–5536, https://doi.org/10.1166/jnn.2016.11743.

[89] C. Mahapatra, R.K. Singh, J.J. Kim, K.D. Patel, R.A. Perez, J.H. Jang, H.W. Kim, Osteopromoting reservoir of stem cells: bioactive mesoporous nanocarrier/collagen gel through slow-releasing fgf18 and the activated bmp signaling, ACS Appl. Mater. Interfaces 8 (2016) 27573–27584, https://doi.org/10.1021/acsami.6b09769.

[90] M.T. Tavares, V.M. Gaspar, M.V Monteiro, J.P.S. Farinha, C. Baleizao, M. Joao F, GelMA /bioactive silica nanocomposite bioinks for stem cell osteogenic differentiation, Biofabrication 13 (2021) 035012, https://doi.org/10.1088/1758-5090/abdc86.

[91] M.T. Tavares, M.B. Oliveira, J.F. Mano, J.P.S. Farinha, C. Baleizão, Bioactive silica nanoparticles with calcium and phosphate for single dose osteogenic differentiation, Mater. Sci. Eng. C 107 (2020) 110348, https://doi.org/10.1016/j.msec.2019.110348.

[92] F. Baino, S. Fiorilli, C. Vitale-Brovarone, Bioactive glass-based materials with hierarchical porosity for medical applications: Review of recent advances, Acta Biomater. 42 (2016) 18–32, https://doi.org/10.1016/j.actbio.2016.06.033.

[93] H. Zhu, K. Zheng, A.R. Boccaccini, Multi-functional silica-based mesoporous materials for simultaneous delivery of biologically active ions and therapeutic biomolecules, Acta Biomater. 129 (2021) 1–17, https://doi.org/10.1016/j.actbio.2021.05.007.

[94] G. Gao, A.F. Schilling, T. Yonezawa, J. Wang, G. Dai, X. Cui, Bioactive nanoparticles stimulate bone tissue formation in bioprinted three-dimensional scaffold and human mesenchymal stem cells, Biotechnol. J. 9 (2014) 1304–1311, https://doi.org/10.1002/biot.201400305.

[95] Á.J. Leite, B. Sarker, T. Zehnder, R. Silva, J.F. Mano, A.R. Boccaccini, Bioplotting of a bioactive alginate dialdehyde-gelatin composite hydrogel containing bioactive glass nanoparticles, Biofabrication 8 (2016) 035005, https://doi.org/10.1088/1758-5090/8/3/035005.

[96] E. Bonnelye, A. Chabadel, F. Saltel, P. Jurdic, Dual effect of strontium ranelate: Stimulation of osteoblast differentiation and inhibition of osteoclast formation and resorption in vitro, Bone 42 (2008) 129–138, https://doi.org/10.1016/j.bone.2007.08.043.

[97] Z. Hong, R.L. Reis, J.F. Mano, Preparation and in vitro characterization of novel bioactive glass ceramic nanoparticles, J. Biomed. Mater. Res. A 88 (2009) 304–313, https://doi.org/10.1002/jbm.a.31848.

[98] V. Guduric, N. Belton, R.F. Richter, A. Bernhardt, J. Spangenberg, C. Wu, A. Lode, M. Gelinsky, Tailorable zinc-substituted mesoporous bioactive glass/alginate-methylcellulose composite bioinks, Materials 14 (2021) 1–21, https://doi.org/10.3390/ma14051225.

[99] X. Wang, E. Tolba, H.C.S. Der, M. Neufurth, Q. Feng, B.R. Diehl-Seifert, W.E. G. Mü Ller, Effect of bioglass on growth and biomineralization of saos-2 cells in hydrogel after 3d cell bioprinting, PLoS One 9 (2014) 1–7, https://doi.org/10.1371/journal.pone.0112497.

[100] M. Ojansivu, A. Rashad, A. Ahlinder, J. Massera, A. Mishra, K. Syverud, A. Finne-Wistrand, S. Miettinen, K. Mustafa, Wood-based nanocellulose and bioactive glass modified gelatin-alginate bioinks for 3D bioprinting of bone cells, Biofabrication 11 (2019) 035010, https://doi.org/10.1088/1758-5090/ab0692.

[101] M. Wang, H. Li, Y. Yang, K. Yuan, F. Zhou, H. Liu, Q. Zhou, S. Yang, T. Tang, A 3D-bioprinted scaffold with doxycycline-controlled BMP2-expressing cells for inducing bone regeneration and inhibiting bacterial infection, Bioact. Mater. 6 (2021) 1318–1329, https://doi.org/10.1016/j.bioactmat.2020.10.022.

[102] E. Karakaya, L. Schöbel, Y. Zhong, J. Hazur, S. Heid, L. Forster, J. Teßmar, A. R. Boccaccini, R. Detsch, How to determine a suitable alginate for biofabrication approaches using an extensive alginate library? Biomacromolecules 24 (2023) 2982–2997, https://doi.org/10.1021/acs.biomac.2c01282.

[103] F. Bider, C. Gunnella, J.T. Reh, C.E. Clejanu, S. Kuth, A.M. Beltrán, A. R. Boccaccini, Enhancing alginate dialdehyde-gelatin (ADA-GEL) based hydrogels for biofabrication by addition of phytotherapeutics and mesoporous bioactive glass nanoparticles (MBGNs), J. Biomater. Appl. 39 (2025) 524–556, https://doi.org/10.1177/08853282241280768.

[104] S. Heid, K. Becker, J. Byun, I. Biermann, Z. Neščáková, H. Zhu, J. Groll, A. R. Boccaccini, Bioprinting with bioactive alginate dialdehyde-gelatin (ADA-GEL) composite bioinks: Time-dependent in-situ crosslinking via addition of calcium-silicate particles tunes in vitro stability of 3D bioprinted constructs, Bioprinting 26 (2022), https://doi.org/10.1016/j.bprint.2022.e00200.

[105] H.H. Lu, C. Froidevaux, I. Biermann, H. Kaňková, M. Büchner, D.W. Schubert, S. Salehi, A.R. Boccaccini, Printable ADA-GEL-based composite inks containing Zn-doped bioactive inorganic fillers for skeletal muscle biofabrication, Biomater. Adv. (2025) 172, https://doi.org/10.1016/j.bioadv.2025.214233.

[106] T. Distler, A.A. Solisito, D. Schneidereit, O. Friedrich, R. Detsch, A.R. Boccaccini, 3D printed oxidized alginate-gelatin bioink provides guidance for C2C12 muscle precursor cell orientation and differentiation via shear stress during bioprinting, Biofabrication 12 (2020), https://doi.org/10.1088/1758-5090/ab98e4.

[107] G. Falcone, S. Schrüfer, S. Kuth, P. Mazzei, S. De Pasquale, P. Del Gaudio, R. P. Aquino, A.R. Boccaccini, P. Russo, Ready-to-print alginate inks: The effect of different divalent cations on Physico-chemical properties of 3D printable alginate hydrogels, Carbohydr. Polym. Technol. Appl. 7 (2024) 100524, https://doi.org/10.1016/J.CARPTA.2024.100524.

[108] K. Loukelis, G. Kontogianni, M. Arango-Ospina, K. Alpantaki, A. Batsali, C. Pontikoglou, A.R. Boccaccini, M. Chatzinikolaidou, 3d bioprinted constructs enriched with zinc-doped bioactive glass promote antibacterial activity and osteochondral tissue regeneration, Adv. Healthcare Mater. 15 (2026) e03186, https://doi.org/10.1002/adhm.202503186.

[109] D. Nieto, J.A. Marchal Corrales, A. Jorge De Mora, L. Moroni, Fundamentals of light-cell-polymer interactions in photo-cross-linking based bioprinting, APL Bioeng. 4 (2020), https://doi.org/10.1063/5.0022693.

[110] V.H. Sánchez-Rodríguez, J.E. Pérez-Cortez, S. Gallegos-Martínez, C. Chuck-Hernández, C.A. Rodriguez, A.R. Boccaccini, E. Vázquez-Lepe, M.M. Alvarez, G. T. de Santiago, J.I. Martínez-López, Light-based and cost-effective bioprinting of musculoskeletal GelMA constructs enriched with mesoporous bioactive glass nanoparticles, Int. J. Bioprint. 10 (2024) 549–564, https://doi.org/10.36922/ijb.1830.

[111] D. Ege, K. Zheng, A.R. Boccaccini, Borate bioactive glasses (BBG): bone regeneration, wound healing applications, and future directions, ACS Appl. Bio Mater. 5 (2022) 3608–3622, https://doi.org/10.1021/acsabm.2c00384.

[112] O.D. Abodunrin, K. El Mabrouk, M. Bricha, A review on borate bioactive glasses (BBG): effect of doping elements, degradation, and applications, J. Mater. Chem. B 11 (2023) 955–973, https://doi.org/10.1039/d2tb02505a.

[113] A.M. Deliormanli, X. Liu, M.N. Rahaman, Evaluation of borate bioactive glass scaffolds with different pore sizes in a rat subcutaneous implantation model, J. Biomater. Appl. 28 (2014) 643–653, https://doi.org/10.1177/0885328212470013.

[114] C. Murphy, K. Kolan, W. Li, J. Semon, D. Day, M. Leu, 3D bioprinting of stem cells and polymer/bioactive glass composite scaffolds for bone tissue engineering, Int. J. Bioprint. 3 (2017) 53–63, https://doi.org/10.18063/IJB.2017.01.005.
[115] K.C.R. Kolan, J.A. Semon, A.T. Bindbeutel, D.E. Day, M.C. Leu, Bioprinting with bioactive glass loaded polylactic acid composite and human adipose stem cells, Bioprinting 18 (2020) e00075, https://doi.org/10.1016/j.bprint.2020.e00075.
[116] M. Vallet-Regí, I. Izquierdo-Barba, A.J. Salinas, Influence of P2O5 on crystallinity of apatite formed in vitro on surface of bioactive glasses, J. Biomed. Mater. Res. 46 (1999) 560–565, https://doi.org/10.1002/(SICI)1097-4636(19990915)46, 4<560::AID-JBM14>3.0.CO;2-M.
[117] C. Duée, I. Grattepanche-Lebecq, F. Désanglois, C. Follet-Houttemane, F. Chai, H. F. Hildebrand, Predicting bioactive properties of phosphosilicate glasses using mixture designs, J. Non. Cryst. Solids 362 (2013) 47–55, https://doi.org/10.1016/j.jnoncrysol.2012.10.033.
[118] A.L. Mîrț, D. Ficai, O.C. Oprea, G. Vasilievici, A. Ficai, Current and Future Perspectives of Bioactive Glasses as Injectable Material, Nanomaterials 14 (2024) 1196, https://doi.org/10.3390/nano14141196.
[119] I. Lebecq, F. Desanglois, A. Leriche, C. Follet-Houttemane, Compositional dependence on the in vitro bioactivity of invert or conventional bioglasses in the Si-Ca-Na-P system, J. Biomed. Mater. Res. A. 83 (2007) 156–168, https://doi.org/10.1002/jbm.a.31228.
[120] Y. Liu, X. Liu, H. Guo, X. Wang, A. Li, D. Qiu, Q. Gu, 3D bioprinting bioglass to construct vascularized full-thickness skin substitutes for wound healing, Mater. Today Bio. 24 (2024) 100899, https://doi.org/10.1016/j.mtbio.2023.100899.
[121] A. Li, D. Qiu, Phytic acid derived bioactive CaO-P2O5-SiO2 gel-glasses, J. Mater. Sci. Mater. Med. 22 (2011) 2685–2691, https://doi.org/10.1007/s10856-011-4464-7.
[122] L. Xu, S. Gao, R. Zhou, F. Zhou, Y. Qiao, D. Qiu, Bioactive pore-forming bone adhesives facilitating cell ingrowth for fracture healing, Adv. Mater. 32 (2020) 1–7, https://doi.org/10.1002/adma.201907491.
[123] H. Zhu, M. Monavari, K. Zheng, T. Distler, L. Ouyang, S. Heid, Z. Jin, J. He, D. Li, A.R. Boccaccini, 3d bioprinting of multifunctional dynamic nanocomposite bioinks incorporating Cu-doped mesoporous bioactive glass nanoparticles for bone tissue engineering, Small 18 (2022) 2104996, https://doi.org/10.1002/smll.202104996.
[124] V. Guduric, J. Wieckhusen, A. Bernhardt, T. Ahlfeld, A. Lode, C. Wu, M. Gelinsky, Composite bioinks with mesoporous bioactive glasses—a critical evaluation of results obtained by in vitro experiments, Front. Bioeng. Biotechnol. 9 (2022) 1–13, https://doi.org/10.3389/fbioe.2021.767256.
[125] A. Hoppe, N.S. Güldal, A.R. Boccaccini, A review of the biological response to ionic dissolution products from bioactive glasses and glass-ceramics, Biomaterials 32 (2011) 2757–2774, https://doi.org/10.1016/j.biomaterials.2011.01.004.
[126] L. Meng, P. Zhao, Y. Jiang, J. You, Z. Xu, K. Yu, A.R. Boccaccini, J. Ma, K. Zheng, Extracellular and intracellular effects of bioactive glass nanoparticles on osteogenic differentiation of bone marrow mesenchymal stem cells and bone regeneration in zebrafish osteoporosis model, Acta Biomater. 174 (2024) 412–427, https://doi.org/10.1016/j.actbio.2023.11.037.
[127] Y. Zhu, X. Zhang, G. Chang, S. Deng, H.F. Chan, Bioactive glass in tissue regeneration: unveiling recent advances in regenerative strategies and applications, Adv. Mater. 37 (2025) 1–16, https://doi.org/10.1002/adma.202312964.
[128] A.I. Damian-Buda, A.R. Boccaccini, Exploring the internalization pathways of silica nanoparticles for targeted intracellular delivery: a discussion of recent results, Biochem. Biophys. Res. Commun. 781 (2025) 152509, https://doi.org/10.1016/j.bbrc.2025.152509.
[129] R. Michel, R. Auzély-Velty, Hydrogel-colloid composite bioinks for targeted tissue-printing, Biomacromolecules 21 (2020) 2949–2965, https://doi.org/10.1021/acs.biomac.0c00305.
[130] N. Mei, Y. Wu, B. Chen, T. Zhuang, X. Yu, B. Sui, T. Ding, X. Liu, 3D-printed mesoporous bioactive glass/GelMA biomimetic scaffolds for osteogenic/cementogenic differentiation of periodontal ligament cells, Front. Bioeng. Biotechnol. 10 (2022) 1–16, https://doi.org/10.3389/fbioe.2022.950970.
[131] T. Jungst, W. Smolan, K. Schacht, T. Scheibel, J. Groll, Strategies and molecular design criteria for 3d printable hydrogels, Chem. Rev. 116 (2016) 1496–1539, https://doi.org/10.1021/acs.chemrev.5b00303.
[132] C. Qin, C. Wu, Inorganic biomaterials-based bioinks for three-dimensional bioprinting of regenerative scaffolds, View 3 (2022) 1–16, https://doi.org/10.1002/VIW.20210018.
[133] V. Bednarzig, S. Schrüfer, T.C. Schneider, D.W. Schubert, R. Detsch, A. R. Boccaccini, Improved 3d printing and cell biology characterization of inorganic-filler containing alginate-based composites for bone regeneration: particle shape and effective surface area are the dominant factors for printing performance, Int. J. Mol. Sci. 23 (2022) 4750, https://doi.org/10.3390/ijms23094750.
[134] D. Chimene, L. Miller, L.M. Cross, M.K. Jaiswal, I. Singh, A.K. Gaharwar, Nanoengineered Osteoinductive bioink for 3d bioprinting bone tissue, ACS Appl. Mater. Interfaces 12 (2020) 15976–15988, https://doi.org/10.1021/acsami.9b19037.
[135] S.A. Wilson, L.M. Cross, C.W. Peak, A.K. Gaharwar, Shear-thinning and thermo-reversible nanoengineered inks for 3d bioprinting, ACS Appl. Mater. Interfaces 9 (2017) 43449–43458, https://doi.org/10.1021/acsami.7b13602.
[136] K. Dubbin, Y. Hori, K.K. Lewis, S.C. Heilshorn, Dual-stage crosslinking of a gel-phase bioink improves cell viability and homogeneity for 3d bioprinting, Adv. Healthc Mater. 5 (2016) 2488–2492, https://doi.org/10.1002/adhm.201600636.
[137] A.-I. Damian-Buda, A.R. Boccaccini, Shedding Light on the Cellular Uptake Mechanisms of Bioactive Glass Nanoparticles as Controlled Intracellular Delivery Platforms: A Review of the Recent Literature, Adv. Healthc. Mater. 15 (2026) e02754, https://doi.org/10.1002/adhm.202502754.
[138] S.C. Pedroza-González, M.P. Pérez González, A.F. Ochoa Tiscareño, P.T. Acosta, R.E. Vargas Mejía, N.A. Ulloa Castillo, M.I. Pérez Valverde, F.J. Sierra, A. R. Valdez, M.M. Boccaccini, G. Alvarez, Santiago Trujillo-de, Synergistic physical and chemical cues enhance cellularization in compartmentalized microchannel fibers supplemented with mesoporous bioactive glass nanoparticles, ACS Mater. Lett 7 (2025) 2765–2775, https://doi.org/10.1021/acsmaterialslett.5c00250.